(12)

Interim Report
on
Grant

N00014-89J-1631

Pseudomorphic Stabilization of Diamond on Non-Diamond Substrates

Part I

Diamond Grown on Single Crystal Beryllium Oxide

A. Argoitia, J.C. Angus, L. Wang*, X.I. Ning* and P. Pirouz*
Chemical Engineering Department
*Materials Science Department

Part II

Anomalous Band Gap Behavior and Phase Stability of c-BN/Diamond Alloys

W.R.L. Lambrecht and B. Segall
Department of Physics

Case Western Reserve University
Cleveland, OH 44106

October 12, 1992

REPORT DOCUMENTATION PAGE

Form Approved
OMB No. 0704-0188

1. AGENCY USE ONLY (Leave blank)	2. REPORT DATE	3. REPORT TYPE AND DATES COVERED
	Oct. 12, 1992	Interim, Jan. 1, 1991 to Sept. 30, 1992

4. TITLE AND SUBTITLE
Pseudomorphic Stabilization of Diamond on Non-Diamond Substrates

5. FUNDING NUMBERS
Grant No. N00014-89J-1631
R&T No. 414s 004-07
Program Element No. 61153N

6. AUTHOR(S)
A. Argoitia, J.C. Angus, L. Wang, X.I. Ning
P. Pirouz, W.R.L. Lambrecht and B. Segall

7. PERFORMING ORGANIZATION NAME(S) AND ADDRESS(ES)
Case Western Reserve University
2040 Adelbert Road
Cleveland, OH 44106

8. PERFORMING ORGANIZATION REPORT NUMBER

9. SPONSORING/MONITORING AGENCY NAME(S) AND ADDRESS(ES)
Office of Naval Research
800 North Quincy Street
Arlington, VA 22217-5660

10. SPONSORING/MONITORING AGENCY REPORT NUMBER

11. SUPPLEMENTARY NOTES
Part I: Diamond Heteroepitaxy on BeO
Part II: Electron Structure Calculations of c-BN/Diamond Alloys

12a. DISTRIBUTION/AVAILABILITY STATEMENT
Approved for public release: Distribution unlimited

12b. DISTRIBUTION CODE

13. ABSTRACT (Maximum 200 words)

Diamond was grown on single crystal beryllium oxide by hot-filament chemical vapor deposition. Individual diamond crystals grew epitaxially on the basal plane of BeO with the epitaxial relationship: $\{111\}_{diamond}$ // $\{0001\}_{BeO}$ and $<1\bar{1}0>_{diamond}$ rotated by less than 6° from $<11\bar{2}0>_{BeO}$.

Electronic structure calculations of mixed crystals of c-BN and diamond show pronounced band gap bowing. The calculations predict only very limited mutual solubility in the solid state.

14. SUBJECT TERMS
Diamond, Chemical Vapor Deposition, Beryllium Oxide, Diamond/c-BN Alloys, Band Gap, Phase Stability

15. NUMBER OF PAGES
47

16. PRICE CODE

17. SECURITY CLASSIFICATION OF REPORT	18. SECURITY CLASSIFICATION OF THIS PAGE	19. SECURITY CLASSIFICATION OF ABSTRACT	20. LIMITATION OF ABSTRACT
Unclassified	Unclassified	Unclassified	UL

DIAMOND GROWN ON SINGLE CRYSTAL BERYLLIUM OXIDE

A. Argoitia and J.C. Angus

Department of Chemical Engineering,
Case Western Reserve University, Cleveland, OH 44106

L. Wang, X. I. Ning, and P. Pirouz

Department of Materials Science and Engineering,
Case Western Reserve University, Cleveland, OH 44106

Submitted to Journal of Applied Physics,
July, 1992

DIAMOND GROWN ON SINGLE CRYSTAL BERYLLIUM OXIDE

A. Argoitia and J.C. Angus

Department of Chemical Engineering,
Case Western Reserve University, Cleveland, OH 44106

L. Wang, X. I. Ning, and P. Pirouz

Department of Materials Science and Engineering,
Case Western Reserve University, Cleveland, OH 44106

ABSTRACT

Diamond has been grown on single crystal beryllium oxide by hot-filament chemical vapor deposition. The diamond particles were characterized by Raman spectroscopy, and the morphology and microstructure investigated by scanning electron microscopy (SEM) and plan-view and cross-sectional transmission electron microscopy (TEM). It has been confirmed that diamond grew epitaxially on the basal plane of BeO with the epitaxial relationship $\{111\}_{diamond}//\{0001\}_{BeO}$ and $<1\bar{1}0>_{diamond}$ rotated by less than 6° with respect to $<11\bar{2}0>_{BeO}$. Diamond was also grown on the $(11\bar{2}0)$ prism plane of BeO. A selected area diffraction pattern obtained from plan-view specimens indicated the presence of a set of spots that corresponded to the $\{10\bar{1}0\}$ planes of hexagonal diamond or to the $\frac{1}{3}(422)$ forbidden spots of cubic diamond. During diamond deposition on $(11\bar{2}0)_{BeO}$ surfaces, small particles of beryllium carbide (Be_2C) were also observed.

I. INTRODUCTION

Diamond films obtained by various chemical vapor deposition techniques are almost all polycrystalline and randomly oriented. However, for electronic applications single crystal films are desirable. Diamond single crystal films with large areas have only been grown successfully by homoepitaxy on single crystal diamond substrates.[1-3] Diamond heteroepitaxy on foreign substrates, e.g., Si[4-6], Ni[7], Cu[8], c-BN[9,10] and β-SiC[11,12], has been limited to small areas.

Cubic BN has a similar structure to diamond and close lattice match (within 2%). However, growth of large single crystal c-BN is probably as difficult as growing large diamond single crystals.

Diamond interfaces with c-BN and BeO have been studied theoretically. These studies show that BeO is, like c-BN, a potentially good substrate for heteroepitaxial growth of diamond. The Be-O bond length in BeO is 0.165 nm, only 7% greater than the C-C bond length of 0.154 nm in diamond. Also, the BeO/diamond adhesion energy was estimated to be 4.6 J/m^2, slightly smaller than that of c-BN/diamond (5.4 J/m^2).[13,14]

One advantage of BeO is that high quality large crystals can be easily grown by a flux process.[15,16] BeO has the wurtzite crystal structure[17] and only by heating to temperatures above 2100°C does it transform to tetragonal beta-beryllia.[18]

The wurtzite crystal structure is based on a h.c.p. lattice with a basis of two atoms per lattice point; Be at (1/3, 2/3, 0) and O at (1/3, 2/3, 3/8) or vice versa. This structure (Table 1) is geometrically similar to Lonsdaleite (hexagonal diamond) and thus the first nearest neighbor positions in BeO are similar to those of cubic diamond. Since the bonding in both diamond and BeO is dominated by nearest neighbor interactions, BeO is a particularly attractive substrate for the heteroepitaxial growth of diamond.

Very different situations for heteroepitaxy are encountered on the different BeO surfaces. The unreconstructed prism planes, e.g., $(11\bar{2}0)$ and $(10\bar{1}0)$, present a situation in which the first and second nearest neighbors are geometrically similar to hexagonal diamond. These surfaces are comprised of six-membered rings in the "boat" conformation, which should presumably favor the heteroepitaxial growth of hexagonal diamond (Fig. 1).

The unreconstructed basal plane surface of BeO is comprised of six-membered rings in the "chair" conformation. The first nearest neighbor interactions are therefore the same for a layer of either cubic or hexagonal diamond. Also, because BeO is non-centrosymmetric, it is a polar crystal and the two basal planes are terminated by beryllium and oxygen. We arbitrarily choose the (0001) surface as beryllium terminated and the $(000\bar{1})$ as oxygen terminated. In an atomic hydrogen environment, the beryllium-terminated basal plane is expected to be more resistant to etching than the oxygen-terminated plane.[19]

II. EXPERIMENTAL

Hot-filament assisted chemical vapor deposition (HFCVD) is one of the most popular methods to grow diamond because of its simplicity, low cost, and ease of scaling up to large surfaces. However, metal contamination from the filament has been detected within the deposited film[20] and in the interfacial layers.[21,22] Much of this contamination comes from the initial heating up of the filament at the beginning of the deposition, perhaps from volatile metal oxides such as WO_x. To reduce contamination, we use a movable molybdenum shutter that can be placed between the filament and the substrate during start-up. Secondary ion mass spectroscopy (SIMS), was used to detect W contamination within a continuous diamond film grown on a scratched silicon wafer. No W contamination was detected either in the bulk of the film or at the interface between the silicon substrate and the film.

Prior to start-up, the molybdenum shutter was placed in between the filaments and substrate. A flow of 100 *sccm* of H_2 at 20 *Torr* was started and the temperature of four filaments connected in series was raised to approximately 2000°C. The temperature of the substrate holder during this procedure was approximately 500°C. Since the shutter was between the filaments and the substrate, the substrate surface was exposed primarily to molecular hydrogen, which cleans the surface of nitrogen, water, hydrocarbons, or any other atmospheric contamination adsorbed by the surface. After ten minutes, a flow of 0.5 *sccm* of CH_4 was started. The shutter was removed 5 minutes later and the distance between the substrate holder and the filaments reduced from 22 *mm* to 5 *mm*. The sample temperature was estimated by a thermocouple at one side of, and at the same level as, the sample. The measured temperature was 850°C. The substrate holder was rotated at 1/3 *rpm* to ensure deposition uniformity.

After deposition, the samples were examined by conventional TEM in a Phillips CM20 scanning transmission electron microscope (STEM) operated at 200 kV. High resolution transmission electron microscopy (HRTEM) was performed in a JEOL 4000EX operated at 400 kV (point-to-point resolution of ~ 0.18 nm at Scherzer defocus). Micro Raman spectroscopy was performed with a Dilor XY modular Raman spectrometer, which has a spatial resolution of approximately 1 μm.

III. RESULTS

A. Diamond growth on $(0001)_{BeO}$

A single crystal of <0001> oriented BeO was provided by Brush Wellman Inc. After verification of its orientation by X-ray Laue reflection, the sample was cut into small pieces (2x2x2 mm^3). The (0001) basal plane was selected for diamond deposition instead of the $(000\bar{1})$ oxygen-terminated plane, because it is expected to be more resistant to attack in an atomic hydrogen environment. We determed the polarity of the crystal using the pyroelectric effect.[19] The samples were polished with 4000 grade SiC paper and cleaned ultrasonically in isopropanol. SEM and Raman spectroscopy were performed after sample removal from the reactor. Figure 2 shows the hexagonal-shaped crystals obtained, a number of which have the same orientation. These oriented crystals presented a strong and narrow Raman line at 1332 cm^{-1} and no broad peak at 1500 cm^{-1} (Fig. 3).

An unreconstructed step along a $<10\bar{1}0>$ direction on the basal plane of a wurtzite structure defines a $\{\bar{2}110\}$ prism plane. Assuming that diamond growth on a stepped (0001) surface of BeO takes place by nucleation at the step followed by lateral growth, one can speculate that the initial deposit may have the hexagonal structure (Fig. 4a). An unreconstructed three layer high step on a $(0001)_{BeO}$ surface presents the same geometrical configuration as boat-boat bicyclodecane (Fig. 4b) proposed as a model precursor species for the nucleation of diamond.[23] Computer simulation of diamond growth from nuclei with two parallel stacking errors, e.g., the boat-boat bicyclodecane shows that rapid growth of a thin crystal of Lonsdaleite with the ABAB... stacking sequence can be achieved in the early stages of diamond growth.[24,25] After the elimination of the surface steps, subsequent growth on this initial layer would presumably be cubic diamond, which is more stable than the hexagonal phase. This may be the reason that

the oriented crystals that we observed in this study are hexagonal in shape but have a cubic Raman signal at 1332 cm^{-1}.

We prepared a $<11\bar{2}0>$ cross-sectional TEM specimen from the BeO (0001) sample for conventional and high resolution TEM. Figures 5a and 5b respectively show a cross-sectional micrograph and the corresponding $[1\bar{1}0]$ zone axis diffraction pattern of cubic diamond with the electron beam approximately parallel to $[11\bar{2}0]_{BeO}$. To reach the $[1\bar{1}0]$ zone axis of diamond it was necessary to tilt -6° around the [0001] direction of BeO. This 6° misorientation between the $[1\bar{1}0]$ zone axis of diamond and the $[11\bar{2}0]$ zone axis of BeO can be observed in Fig. 5c, which shows the selected area diffraction pattern of the diamond/BeO interface. The black arrows in this figure identify the 111 diffraction spots of diamond. A set of weak spots (white arrows) corresponding to 0001 BeO diffraction spots planes are located along one set of 111 diffraction spots of diamond. No other structure has been found at the interface between the diamond particle and BeO.

These results show that the diamond particle in Fig. 5a has grown epitaxially on BeO such that the (111) planes of diamond are closely parallel to the {0001} planes of BeO and $<1\bar{1}0>_{diamond}$ is rotated by -6° with respect to $<11\bar{2}0>_{BeO}$. No microstructural details can be seen in Fig. 5a because the diamond particle is too thick.

The same sample was further treated by ion milling to get a thinner interface for high resolution TEM. Figure 6a is a TEM micrograph of the same single crystal diamond grain shown in Fig. 5a. At the top left corner of this micrograph, a micro-twin band can be observed that lies on (111) diamond planes parallel to the (0001) BeO surface. The diffraction pattern, Fig. 6b, from this corner clearly shows one set of twin spots (white arrows) located at one-third of the distance between the transmitted beam and the primary spots from the untwinned diamond; this is typically observed in CVD diamond films.[26] Figure 6c shows an HRTEM image of the diamond. Since the diamond grain is in a $[1\bar{1}0]$ orientation, two sets of {111} fringes with 0.206 *nm* spacing are visible. Note that micro-twins are only present with their (111) habit planes parallel to the (0001) surface of BeO. The 6° misorientation between the $[1\bar{1}0]_{diamond}$ and the $[11\bar{2}0]_{BeO}$ zone axis makes it impossible to obtain a good HRTEM image of BeO and diamond simultaneously, and thus also from the BeO/diamond interface.

Tilting the specimen to the [11$\bar{2}$0] zone axis of BeO (Fig. 6d) made it possible to observe the (1$\bar{1}$00) and (0001) fringes of BeO with 0.234 *nm* and 0.438 *nm* spacings, respectively. The (1$\bar{1}$1) diamond planes visible in Fig. 6d form an angle of ~70° with the (0001) planes of BeO. This corresponds to the angle between {111} crystallographic planes of cubic diamond (70°32') and shows that the (111) diamond planes are parallel to the BeO (0001) basal plane.

Similar results have been obtained with another <11$\bar{2}$0> cross-sectional TEM specimen prepared under the same conditions. Figure 7a shows a cross-sectional micrograph of a diamond particle grown on the basal plane of BeO. In this micrograph the diamond particle is connected to the BeO substrate only at its periphery with its center separated from the basal plane; the bright contrast at the interface forms an angle of approximately 5°. Some micro-twins bands parallel to the BeO surface can also be observed in the right hand side of the diamond particle. A selected area diffraction pattern (Fig. 7b) was obtained from the right hand interface between the diamond particle and the BeO substrate. This diffraction pattern corresponds to a <110> zone axis of cubic diamond with the electron beam tilted less that 3° with respect to $<11\bar{2}0>_{BeO}$. A set of spots (black arrows), corresponding to $\{0001\}_{BeO}$ planes, form an angle of ~8° with one set of 111 spots of cubic diamond (white arrows). We believe that at the early stages of growth, the diamond particle has grown with one of its (111) planes parallel to the $(0001)_{BeO}$ surface. During the process, internal stress produced the separation between the diamond particle and the surface to form the angle of 8°.

The epitaxial relationship found corresponds to the ideal superposition of the (111) planes of diamond on top of the (0001) basal planes of BeO as show in the model presented in Fig. 8. Here it is assumed that the carbon atoms are bonded to the Be atoms at the interface.

B. Diamond growth on $(11\bar{2}0)_{BeO}$

A single crystal sample of BeO with a (11$\bar{2}$0) surface, also obtained from Brush Wellman Inc., was prepared for plan-view TEM prior to diamond deposition. Several 3x3 mm^2 sections were cut from the original (11$\bar{2}$0) oriented sample after verification of its orientation by X-ray Laue reflection. The substrates were then mechanically thinned to a thickness of 100 μm

using a final polish with 4000 grade SiC paper. They were then dimpled to a thickness of 30 μm at the central region. Finally, ion-milling from both sides of the substrate with 5 kV Ar^+ produced a hole at the center of the sample. At this stage the samples were introduced to the CVD reactor. The deposition conditions were the same as those used for $(0001)_{BeO}$ substrate; only the deposition time was shorter (4 hours) in order to study the initial stages of nucleation. Figure 9 shows a SEM micrograph of one of the samples prepared in this way after Au sputtering to avoid charging of the insulating BeO substrate. Only diamond particles grown in the thinner regions of the substrate were useful for TEM studies. This micrograph also shows that the surface of the sample is rough and stepped, and thus it is possible that some of the diamond particles did not grow directly on the $(11\bar{2}0)$ plane of BeO.

A dark-field image of a diamond particle is observed in Fig. 10a with the corresponding selected area diffraction (SAD) pattern (Fig. 10b) obtained from the top corner of the diamond. The beam direction in this figure is parallel to the $[11\bar{2}0]$ zone axis of BeO. The arrowed spots in Fig. 10b identify the $(1\bar{1}00)$, $(1\bar{1}01)$, (0001) and (0002) planes of BeO and the white ones correspond to one set of {111} planes of cubic diamond. The extra spots observed in this figure come from double diffraction when the original electron beam is diffracted by some of the {111} planes of the diamond particle on top of BeO. The geometry is such that the diffracted beams from the diamond particle are incident on some of the BeO planes at the Bragg angle. Effectively, these extra spots disappeared when the specimen was tilted a few degrees about the axis connecting the 111 spots of cubic diamond. Under these conditions, the extra spots in this diffraction pattern formed a similar dark-field image as the one shown in Fig. 10a.

The same diamond particle was tilted so that the beam direction was parallel to the [111] zone axis. The corresponding diffraction pattern is shown in Fig. 10c. The six strong spots around the transmitted spot correspond to {220} planes of cubic diamond (d = 0.126 nm). Figure 10d shows a dark-field image of the diamond obtained from one of these strong spots. The three black-arrowed spots in Fig. 10c correspond to the $(1\bar{1}00)$, $(\bar{1}100)$ and $(01\bar{1}3)$ planes of BeO. In addition, six weak spots (white arrows) appear around the direct spot. From their spacing (d = 0.219 nm), these could be assigned to $10\bar{1}0$ spots from hexagonal diamond or to the

$\frac{1}{3}$(422) forbidden spots from cubic diamond. The latter could occur because of incomplete unit cells at the {111} surfaces of diamond.[27] As mentioned before, the unreconstructed $(11\bar{2}0)$ prism plane presents a "boat" structure favorable for the heteroepitaxial growth of hexagonal diamond. In this case a buffer layer of hexagonal diamond may grow at the surface of BeO before a cubic diamond structure starts growing. Future work, e.g., cross-sectional specimens, will be necessary to confirm the presence of this buffer layer.

Small particles of beryllium carbide (Be_2C) were also present in this sample. Figure 11a shows a SAD pattern obtained from a Be_2C particle. The 020, 220 and 200 diffraction spots of Be_2C are indicated by black arrows, while the white arrows identify the 0001, $\bar{1}100$ and $\bar{1}101$ diffraction spots of BeO. This indicates that the electron beam is parallel to the [001] direction of Be_2C and the $[11\bar{2}0]$ direction of BeO. Figure 11b shows a dark field image of the Be_2C particle. Note that some small Be_2C particles also light up. The structure of the small particles has been also confirmed by the HRTEM micrograph shown in Fig. 11c where the $(10\bar{1}0)$ and (0001) fringes of BeO with 0.234 *nm* and 0.438 *nm* spacing, respectively, are observed. The Be_2C particle shown is in a [110] orientation and two sets of $\{1\bar{1}1\}$ fringes with 0.247 *nm* spacing are visible. Beryllium carbide has the antifluorite structure (Table 1) and is easily hydrolyzed by contact with moist air to form $Be(OH)_2$ at room temperature.[28,29] Its presence indicates that Be_2C can be stable in small quantities, or when it is protected by a very thin layer of another material. In any case, its formation should be avoided for diamond heteroepitaxy because its presence is not favorable for this purpose.

IV. CONCLUSIONS

The conclusions can be summarized as follows:

(i) Diamond particles were grown heteroepitaxially on the basal plane of BeO with an epitaxial relationship $\{111\}_{diamond}$ // $\{0001\}_{BeO}$ and $<1\bar{1}0>_{diamond}$ rotated by less than 6° with respect to $<11\bar{2}0>_{BeO}$. Since large crystals of BeO can be grown, this material is a potential substrate for growing diamond single crystals, or highly oriented diamond films.

(ii) HRTEM image and SAD patterns of the diamond/BeO interface show that, under the conditions utilized, no interfacial phases form during the deposition of diamond on BeO.

(iii) No epitaxial relationship has been found when diamond is grown on $(11\bar{2}0)_{BeO}$.

(iv) Small particles of Be_2C have been found when diamond is grown on the $(11\bar{2}0)$ prism plane of BeO.

(v) SAD pattern of diamond grown on the $(11\bar{2}0)$ prism plane of BeO shows the presence of weak spots that can be assigned to either the forbidden $\frac{1}{3}(422)$ spots of cubic diamond, or the $10\bar{1}0$ diffraction spots of hexagonal diamond.

ACKNOWLEDGMENTS

The BeO single crystals were supplied by Dr. Jere Brophy of Brush Wellman Inc. The Raman spectroscopy was performed by Dr. Yaxin Wang. Mr. Mahendra Sunkara supplied the crystal models. The support of the Office of Naval Research, grant N00014-89J-1631 and the National Science Foundation Materials Research Group, grant DMR 89-03527 is gratefully acknowledged.

REFERENCES

1. B. V. Derjaguin, B. V. Spitsyn, A. E. Gorodetsky, A. P. Zakharov, L. I.Bouilov and A. E. Aleksenko, J. Crystal Growth 31, 44 (1975).

2. H. Nakazawa, Y. Kanazawa, M. Kamo and K. Osumi, Thin Solid Films 151, 199 (1987).

3. M. W. Geis, presented at the Third Annual SDIO/IST-ONR Diamond Technology Initiative Symposium, Crystal City, VA, July (1988).

4. J. Narayan, A. R. Srivatsa, M. Peters, S. Yokota and K. V. Ravi, Appl. Phys. Lett. 53, 1823 (1988).

5. B. E. Williams and J. T. Glass, J. Mater.Res., 4, 373 (1989).

6. D. G. Jeng, H. S. Tuan, R. F. Salat and G. J. Fricano, Appl. Phys. Lett. 20, 1868 (1990).

7. Y. Sato, I. Yashima, H. Fujita, T. Ando and M. Kamo, Proceedings of Second International Conference on the New Diamond Science and Technology, Washington, D.C., Sept. 23-27, 1990, R. Messier, J. T. Glass, J. E. Butler and R. Roy, Editors, Materials Research Society, Pittsburgh, PA, p. 371 (1991).

8. J. F. Prins, Proceedings of Second International Conference on the New Diamond Science and Technology, Washington, D.C., Sept. 23-27, 1990, R. Messier, J. T. Glass, J. E. Butler and R. Roy, Editors, Materials Research Society, Pittsburgh, PA, p. 386 (1991).

9. W. E. Pickett, Phys. Rev. B 38, 1316 (1988).

10. S. Koizumi, T. Murakami and T. Inuzuka, Appl. Phys. Lett. 6, 563 (1990).

11. W. Wang, K. Liao and J. Gao, Phys. Stat. Sol. (a) 128, K83 (1991).

12. B. R. Stoner and J. T. Glass, Appl. Phys. Lett. 6, 698 (1992).

13. W. R. L. Lambrecht and B. Segall, Phys. Rev. B. 40, 9909 (1989); Phys. Rev. B 41, 5409 (1990).

14. W. R. L. Lambrecht and B. Segall, J. Mater. Res. 7, 696 (1992).

15. S. B. Austerman. J. Nuclear Mat. 14, 225 (1964).

16. S. B. Austerman. J. Cryst. Growth 42, 284 (1977).

17. C. F. Cline and J. S. Kahn, J. Electrochem. Soc. 110, 773 (1963).

18. D. K. Smith, C. F. Cline and S. B. Austerman, J. Nuclear Mat. 14, 237 (1964).

19. S. B. Austerman, D. A. Berlincourt and H. H. A. Krueger, J. Appl. Physics. 34, 2, 339 (1963).

20. H. J. Hinneberg, M. Eck and K. Schmidt, Diamond and Diamond Like Related Coatings, Sep. 2-6, 1991 Nice, France. To be published, Elsevier, Amsterdam.

21. E. Gheeraert, A. Deneuville, L. Brunel and J. C. Oberlin, Diamond and Diamond Like Related Coatings, Sep. 2-6, 1991 Nice, France. To be published, Elsevier, Amsterdam.

22. G. H. M. Ma, Y. H. Lee and J. T. Glass, J. Mater. Res, 5, 2367 (1990).

23. J. C. Angus, R. W. Hoffman, and P. H. Schmidt, Science and Technology of New Diamond, Proceedings of the First Int. Conf. on the New Diamond Science and Technology, Tokyo, 1988; KTK Scientific Publishers/Terra Scientific Publishing. S. Saito, O. Fukunaga, and M. Yoshikama, Editors, p. 9 (1990).

24. J. C. Angus, Z. Li, M. Sunkara, R. Gat, A. B. Anderson, S. P. Mehandru, and M. W. Geis, Proceedings of the Second International Symposium on Diamond Materials, Washington, D.C., May 5-10, 1991. A. J. Purdes, J. C. Angus, R. F. Davis, B. M. Meyerson, K. E. Spear, and M. Yoder, Editors, Electrochemical Society, Pennington, N.J., p. 125, (1991)

25. J. C. Angus, M. Sunkara, S. Sahaida and J. T. Glass, Submitted to J. Mat. Res. (1992).

26. J. C. Walmsley, Presented at Microsc. Semicond. Mater. Conf., Oxford, 10-13 April 1989. Inst. Phys. Conf. Series. 100, 3 (1989).

27. R. H. Morris, W. R. Bottoms and R. G. Peacock, J. Appl. Phys. 39, 3016 (1968).

Material	Diamond	BeO	Lonsdaleite	Be_2C
Symmetry	Cubic	Hexagonal (Wurzite)	Hexagonal	Cubic (Antifluorine)
Space Group	Fd3m	P63mc	P63mmc	Fm3m
C-C bond length (*nm*)	0.154		0.154	
Be-O bond length (*nm*)		0.165		
Be-C bond length (*nm*)				0.187
Lattice parameters (*nm*)	a=0.3567	a=0.2696 c=0.4379	a=0.252 c=0.412	a=0.433

Table 1. Crystal structure data for diamond, lonsdaleite, beryllium oxide and beryllium carbide

28. J. H. Coobs and W. J. Koshuba, J. Electrochem. Soc. 99, 115 (1952).

29. M. W. Mallett, E. A. Durbin, M. C. Udy, D. A. Vaughan and E. J. Center. J. Electrochem. Soc. 101, 298 (1954).

FIGURE CAPTIONS

Figure 1. Crystallographic model of the ideal heteroepitaxial growth of hexagonal diamond on the $(11\bar{2}0)$ surface of BeO. Grey, white and black balls are respectively carbon, oxygen and beryllium atoms. It is assumed that C is bonded to Be at the interface.

Figure 2. Hexagonal-shaped diamonds, some showing the same orientation, grown on the (0001) basal plane of BeO.

Figure 3. Raman signal of cubic diamond particles shown in Fig. 2.

Figure 4. (a) Crystallographic model representing an initial deposit of hexagonal diamond on an unreconstructed three layer step of $(0001)_{BeO}$. Grey, white and black balls are respectively carbon, oxygen and beryllium atoms.

(b) Boat-boat bicyclodecane with two parallel stacking errors. Positions of two carbon ad-atoms are shown as black circles.

Figure 5. (a) $<11\bar{2}0>_{BeO}$ cross-sectional TEM micrograph of diamond on BeO.

(b) $[1\bar{1}0]$ zone axis diffraction pattern of the diamond single crystal shown in Fig. 5a.

(c) $[1\bar{1}0]_{diamond}$ SAD pattern from the BeO/diamond interface shown in Fig. 5a.

Figure 6. (a) TEM micrograph of the diamond grain shown in Fig. 5a after further ion milling.

(b) Set of twin spots between the 111 diamond diffraction spots corresponding to the plane parallel to the (0001) BeO surface.

(c) HRTEM image of the [110] oriented diamond. $\{1\bar{1}1\}$ fringes with 0.206 *nm* spacing are visible in the diamond.

(d) HRTEM image of the $[11\bar{2}0]$ oriented BeO where traces of

$(1\bar{1}00)$ and (0001) planes with 0.234 *nm* and 0.438 *nm* spacing, respectively, are visible. The $(1\bar{1}\bar{1})$ diamond planes form an angle of ~70° with the (0001) planes of BeO.

Figure 7. Crystallographic model of the ideal superposition of (111) diamond on top of the (0001) basal planes of BeO. Grey, white and black balls are respectively carbon, oxygen and beryllium atoms.

Figure 8. (a) $<11\bar{2}0>_{BeO}$ cross-sectional TEM micrograph of diamond on BeO.

(b) $[1\bar{1}0]_{diamond}$ SAD pattern from the BeO/diamond interface. Black arrows denote BeO 0001 diffraction spots. White arrows denote 111 diffraction spots from cubic diamond. The angle between $(0001)_{BeO}$ and $(111)_{diamond}$ is approximately 8°.

Figure 9. SEM micrograph of a $(11\bar{2}0)_{BeO}$ plan-view TEM sample after diamond deposition.

Figure 10. (a) Dark-field image of diamond grown on $(11\bar{2}0)$ surface of BeO.

(b) SAD pattern obtained with the electron beam parallel to $[11\bar{2}0]$ zone axis of BeO. Black-arrowed spots identify the $(1\bar{1}00)$, $(1\bar{1}01)$, (0001) and (0002) planes of BeO; the white arrows denote correspond to one set of {111} planes of cubic diamond. The extra spots observed in this figure come from double diffraction.

(c) Diffraction pattern of diamond shown in Fig. 10a tilted to its [111] zone axis. The six strong spots correspond to the $\{2\bar{2}0\}$ planes of cubic diamond. The three black-arrowed spots are from BeO and the six weak spots (white-arrowed) can be assigned as $10\bar{1}0$ of hexagonal diamond or the $\frac{1}{3}(422)$ forbidden spots of cubic diamond.

(d) Dark-field image of the diamond obtained with one of the $\{2\bar{2}0\}$ planes shown in Fig. 10c.

Figure 11. (a) SAD pattern obtained from the large Be_2C particle shown in Fig. 11b. Black arrows denote the 020, 220 and 200 diffraction spots of Be_2C. White arrows denote the 0001, $\bar{1}100$ and $\bar{1}101$ diffraction spots of BeO.

(b) Dark field image of Be_2C formed from one of the black-arrowed spot shown in Fig. 11a.

(c) HRTEM micrograph of a small Be_2C particle on BeO showing the $(10\bar{1}0)$ and (0001) fringes of BeO with 0.234 *nm* and 0.438 *nm* spacing respectively and two sets of $(1\bar{1}1)$ fringes of Be_2C with 0.247 *nm* spacing.

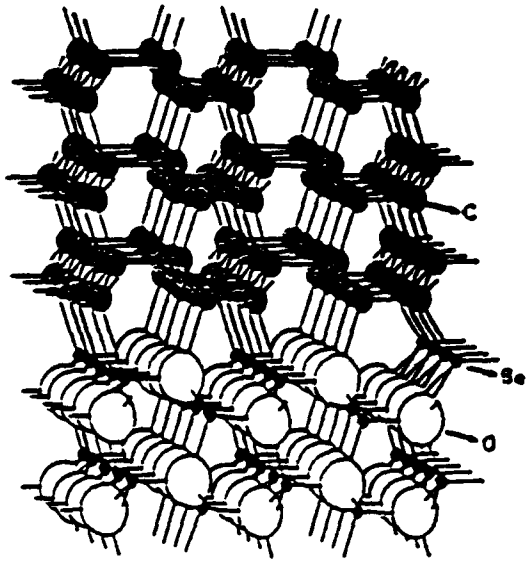

Figure 1. Crystallographic model of the ideal heteroepitaxial growth of hexagonal diamond on the (11$\bar{2}$0) surface of BeO. Grey, white and black balls are respectively carbon, oxygen and beryllium atoms. It is assumed here that C is bonded to Be at the interface.

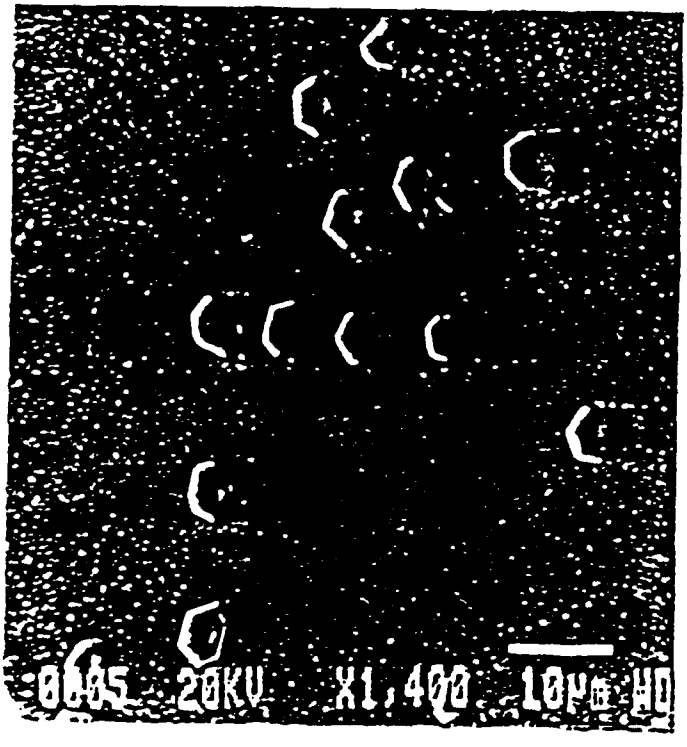

Figure 2. Hexagonal-shaped diamonds, some showing the same orientation, grown on the (0001) basal plane of BeO.

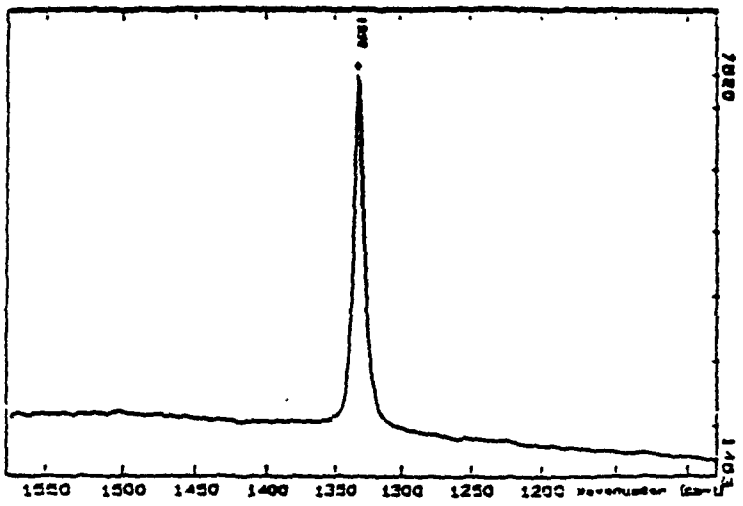

Figure 3. Raman signal of cubic diamond particles shown in Fig. 2.

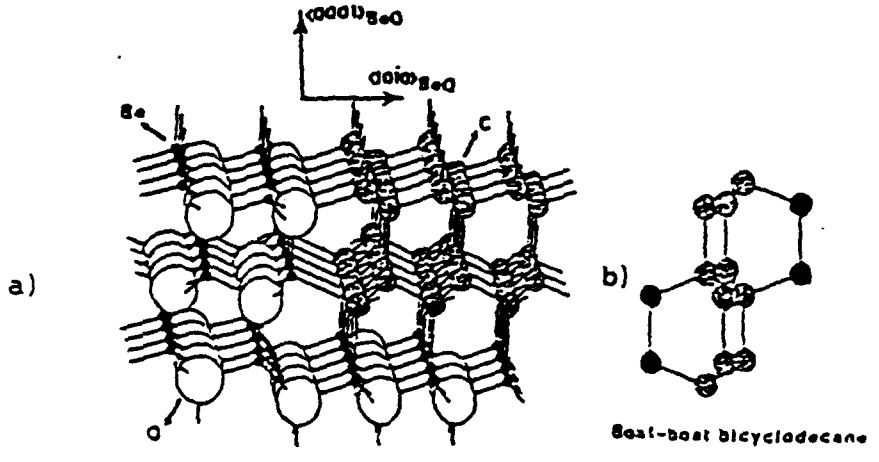

Figure 4. (a) Crystallographic model representing an initial deposit of hexagonal diamond on an unreconstructed three layer step of $(0001)_{BeO}$. Grey, white and black balls are respectively carbon, oxygen and beryllium atoms.
(b) Boat-boat bicyclodecane with two parallel

Figure 5. (a) $<11\bar{2}0>_{BeO}$ cross-sectional TEM micrograph of diamond on BeO.

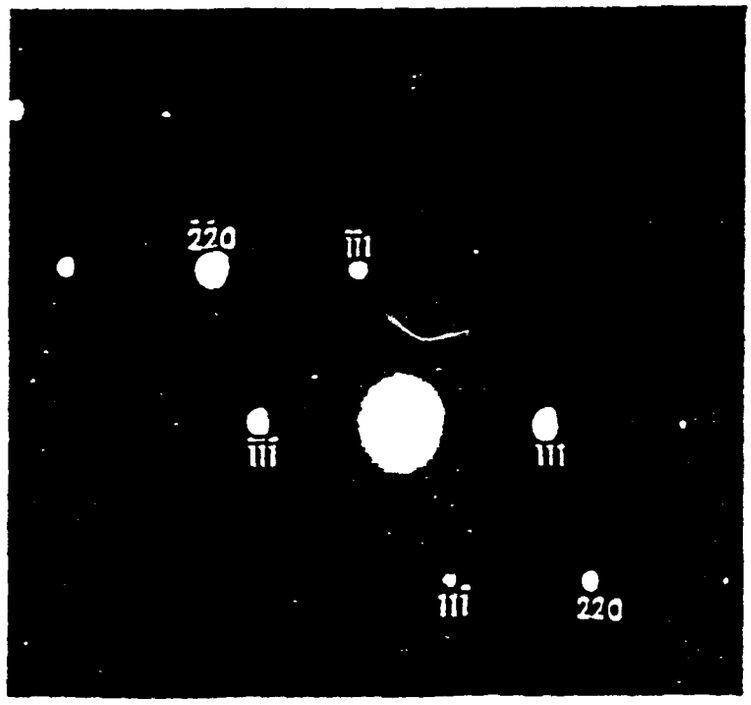

Figure 5. (b) $[1\bar{1}0]$ zone axis diffraction pattern of the diamond single crystal shown in Fig. 5a.

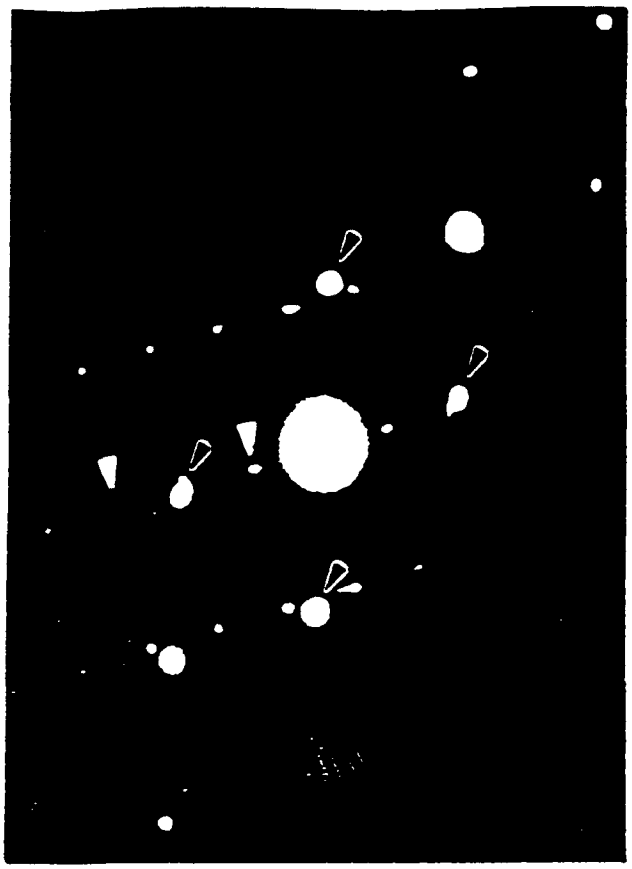

Figure 5. (c) $[1\bar{1}0]_{diamond}$ SAD pattern from the BeO/diamond interface shown in Fig. 5a.

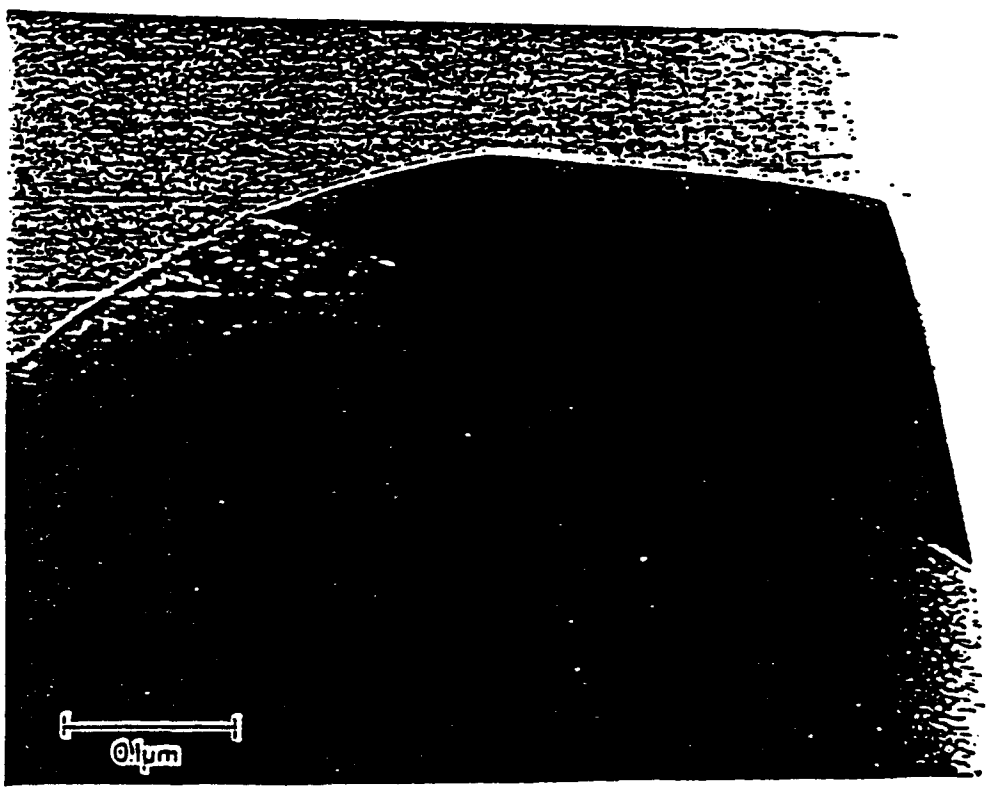

Figure 6. (a) TEM micrograph of the diamond grain shown in Fig. 5a after further ion milling.

Figure 6. (b) Set of twin spots between the 111 diamond diffraction spots corresponding to the plane parallel to the (0001) BeO surface.

Diamond
2.06 Å
BC8

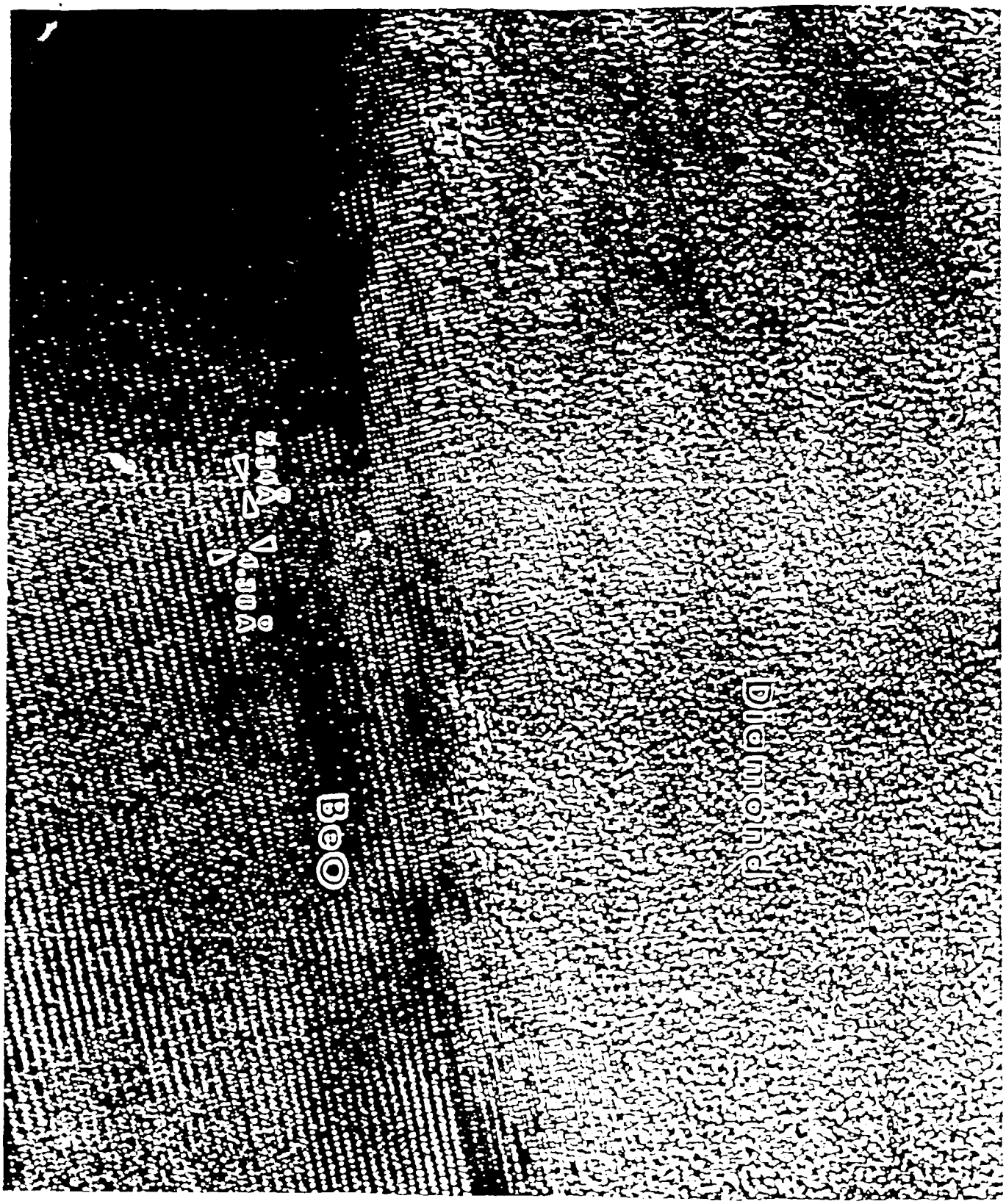

Figure 6. (d) HRTEM image of the [11$\bar{2}$0] oriented BeO where traces of (1$\bar{1}$00) and (0001) planes with 0.234 *nm* and 0.438 *nm* spacing, respectively, are visible. The (1$\bar{1}$1) diamond planes form an angle of ~70° with the (0001) planes of BeO.

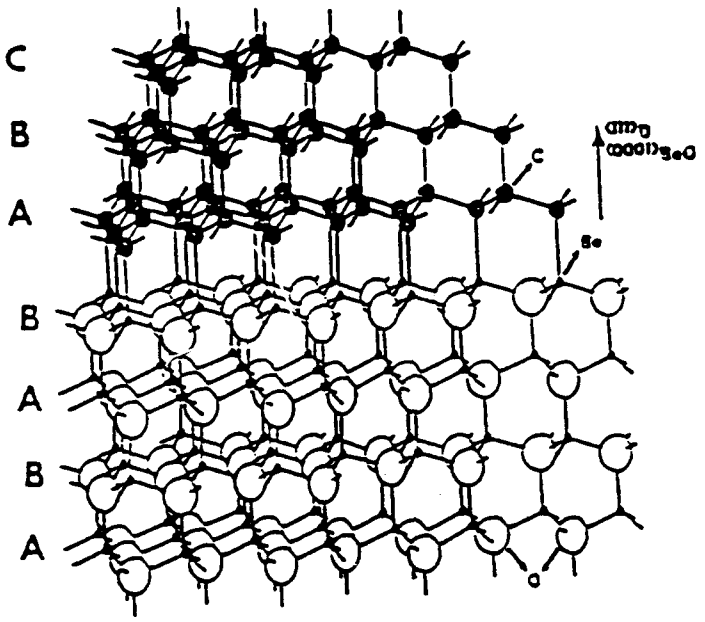

Figure 7. Crystallographic model of the ideal superposition of (111) diamond on top of the (0001) basal planes of BeO. Grey, white and black balls are respectively carbon, oxygen and beryllium atoms.

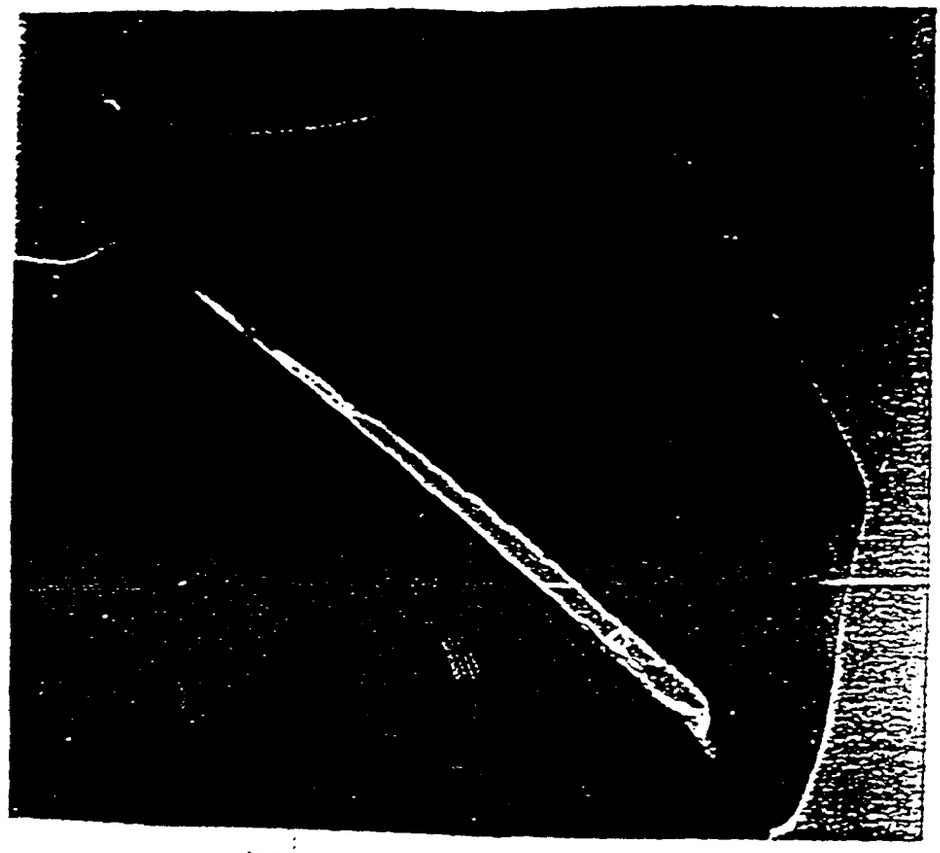

Figure 8. (a) $<11\bar{2}0>_{BeO}$ cross-sectional TEM micrograph of diamond on BeO.

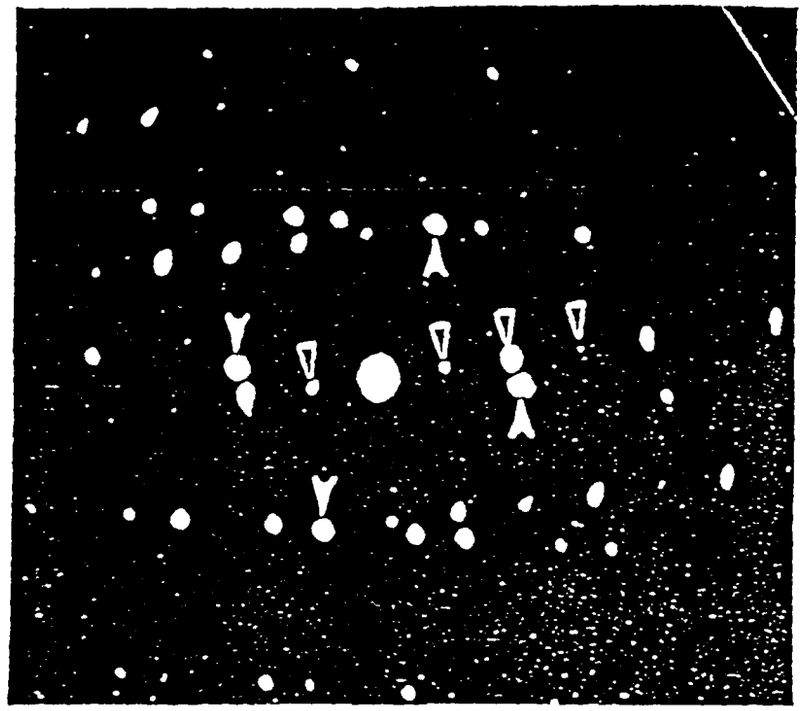

Figure 8. (b) $[1\bar{1}0]_{diamond}$ SAD pattern from the BeO/diamond interface. Black arrows denote BeO 0001 diffraction spots. White arrows denote 111 diffraction spots from cubic diamond. The angle between $(0001)_{BeO}$ and $(111)_{diamond}$ is approximatly 8º.

Figure 9. SEM micrograph of a $(11\bar{2}0)_{BeO}$ plan-view TEM sample after diamond deposition.

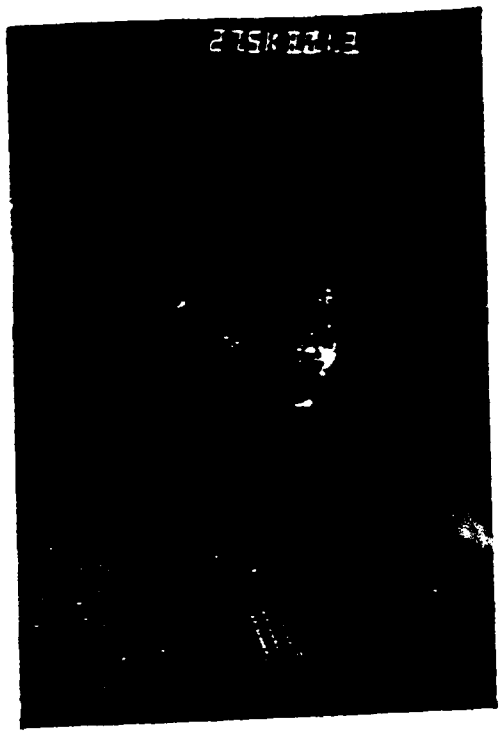

Figure 10. (a) Dark-field image of diamond grown on (11$\bar{2}$0) surface of BeO.

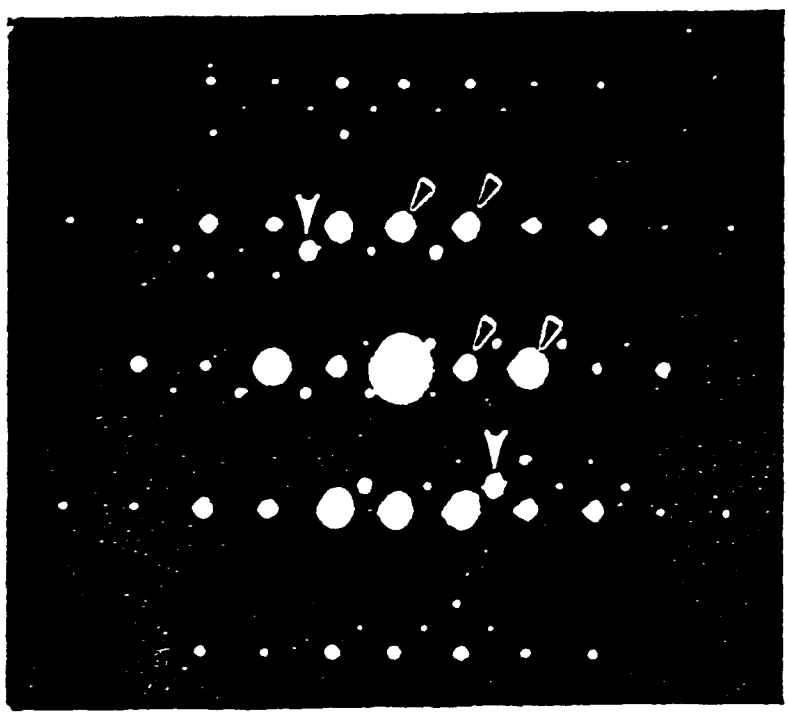

Figure 10. (b) SAD pattern obtained with the electron beam parallel to [11$\bar{2}$0] zone axis of BeO. Black-arrowed spots identify the (1$\bar{1}$00), (1$\bar{1}$01), (0001) and (0002) planes of BeO; the white ones correspond to one set of {111} planes of cubic diamond. The extra spots observed in this figure come from double diffraction.

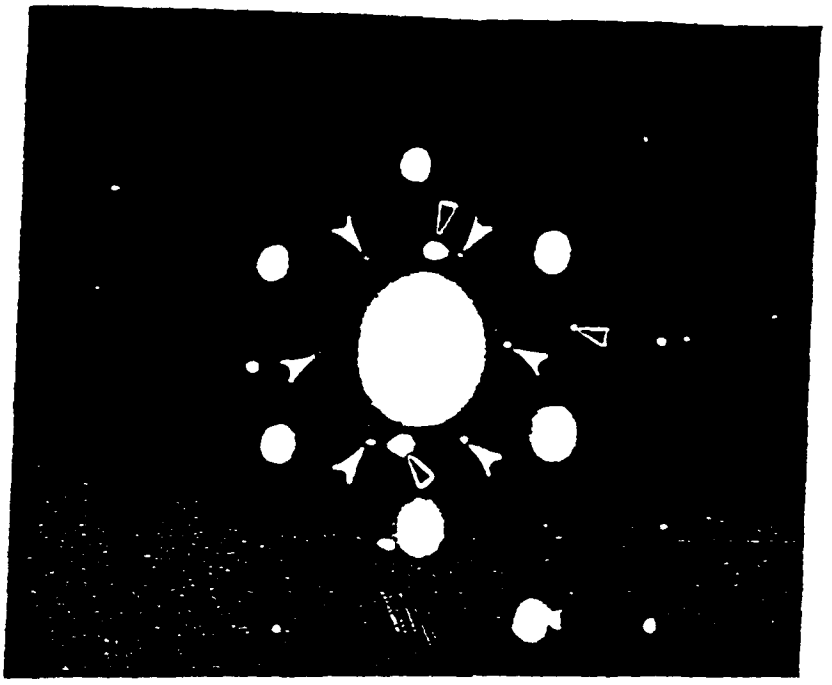

Figure 10. (c) Diffraction pattern of diamond shown in Fig. 10a tilted to its [111] zone axis. The six strong spots correspond to the $\{2\bar{2}0\}$ planes of cubic diamond. The three black-arrowed spots are from BeO and the six weak spots (white-arrowed) can be assigned as $10\bar{1}0$ of hexagonal diamond or $\frac{1}{3}(422)$ forbidden spots of cubic diamond.

Figure 10. (d) Dark-field image of the diamond obtained with one of the $\{2\bar{2}0\}$ planes shown in Fig. 10c.

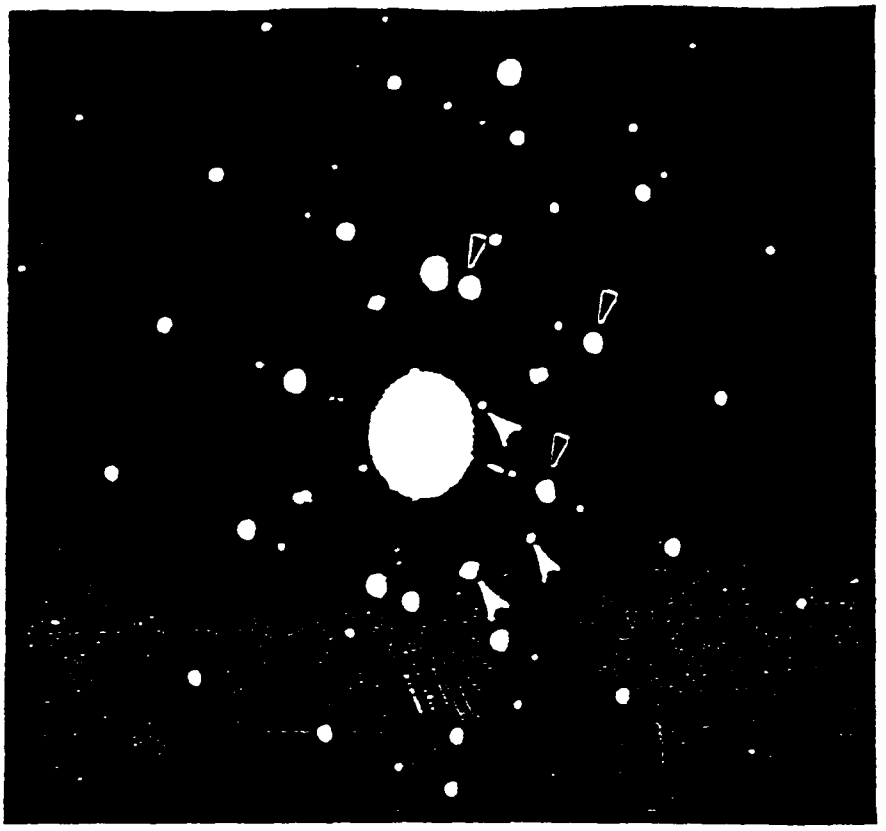

Figure 11. (a) SAD pattern obtained from the large Be_2C particle shown in Fig.11b. Black arrows denote the 020, 220 and 200 diffraction spots of Be_2C. White arrows denote the 0001, ($\bar{1}100$) and ($\bar{1}101$) diffraction spots of BeO.

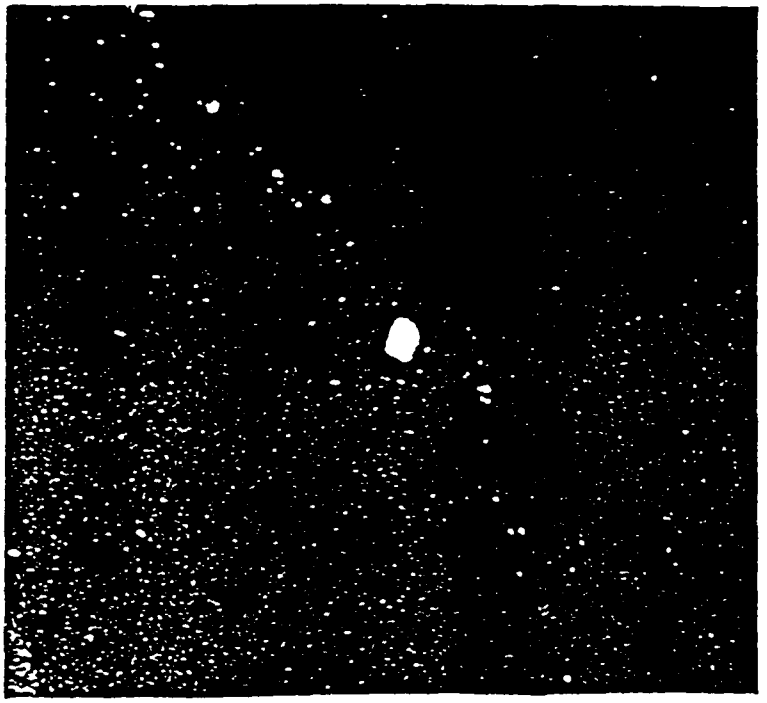

Figure 11. (b) Dark field image of Be_2C formed from one of the black-arrowed spot shown in Fig. 11a.

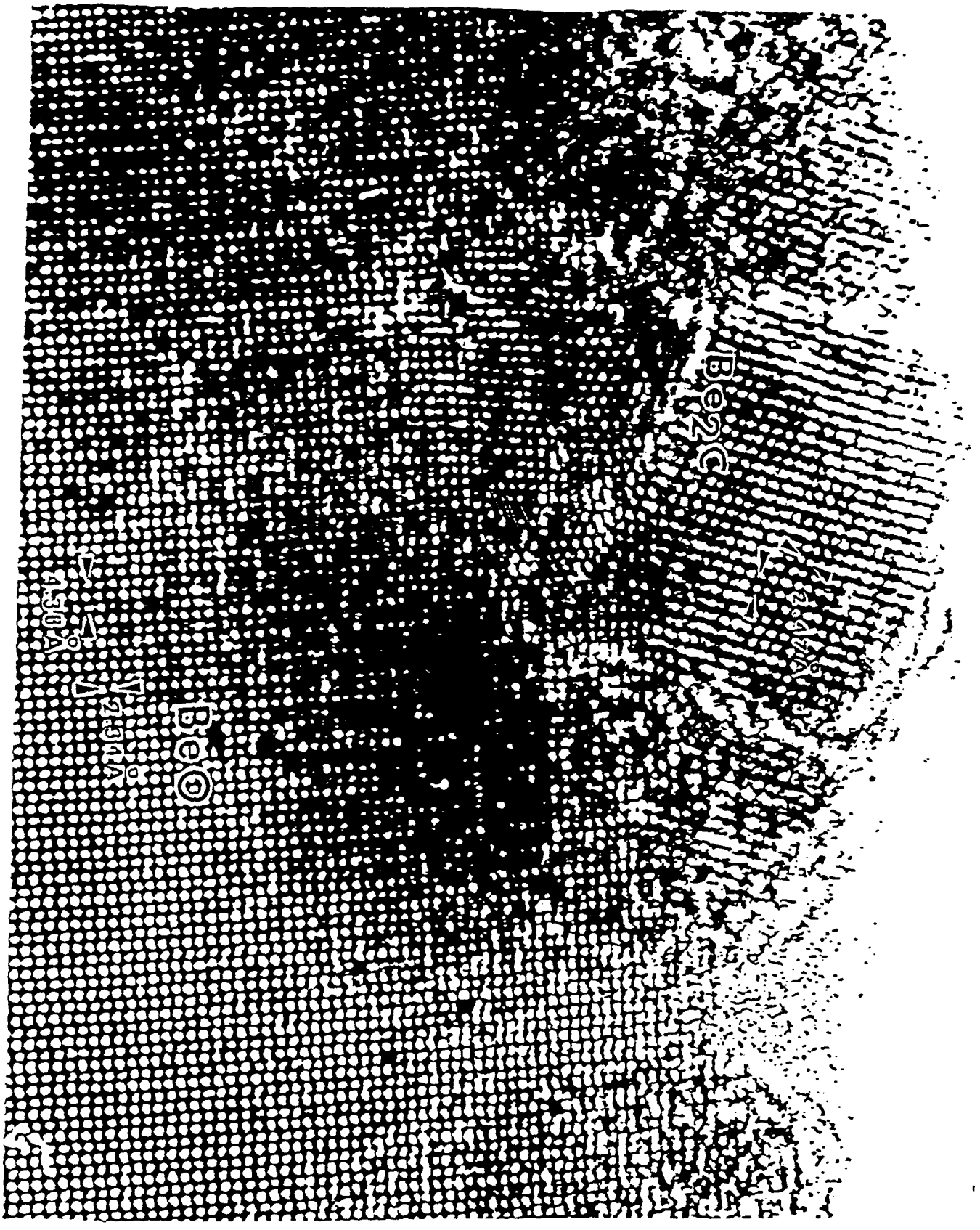

Figure 11. (c) HRTEM micrograph of a small Be_2C particle showing the $(10\bar{1}0)$ and (0001) fringes of BeO with 0.234 *nm* and 0.438 *nm* spacing respectively and two sets of $(1\bar{1}1)$ fringes of Be_2C with 0.247 *nm* spacing.

Preprint Submitted to Phys. Rev. B Manuscript No. BX4550

Anomalous band-gap behavior and phase stability of c-BN–diamond alloys

Walter R. L. Lambrecht and Benjamin Segall
Department of Physics, Case Western Reserve University, Cleveland, OH 44106-7079
(Received October 6, 1992)

Electronic structure calculations predict that hypothetical ordered mixed crystals of c-BN and diamond-C representative of the expected short-range order in the alloys show a very pronounced band-gap bowing. This anomalous behavior is believed to be related to the staggered band line-up at the corresponding heterojunction. The miscibility phase diagram of this system is estimated using a simple pseudobinary "regular solution" model for the short-range order and the energies of formation of the representative ordered compounds calculated from first-principles. It indicates that there is only very limited mutual solubility in the solid state. The bandgaps and energies of formation of the disordered ternary alloys are estimated by means of cluster expansions.

PACS: 71.25.Tn, 61.55Hg

I. INTRODUCTION

Diamond and c-BN have recently received considerable attention because of their promising materials properties for abrasives, heatsinks, protective coatings and even wide-band-gap semiconductor applications. This interest stems from the extreme values of these two materials' properties such as hardness, thermal conductivity, elastic constants, and band gaps [1]. The recent interest has surged as a result of the increased availability of these difficult to obtain materials. This in turn resulted from the development of a number of novel growth techniques among which are energetically enhanced (plasma, hot-filament, microwave) chemical vapor deposition (CVD) [2], laser ablation [3] and ion beam techniques [4]. A basic difficulty common to both materials is that they are thermodynamically only stable at high pressures, the low-pressure ground states being the layered hexagonal phases: graphite and h-BN.

Mixed C-BN layered hexagonal phases have been synthesized by a number of groups [5–7] and studied theoretically by Liu et al. [8]. Badzian [5] has synthesized mixed crystals of diamond and c-BN by a high-pressure high temperature phase transformation technique starting from the layered hexagonal mixed crystals. Attempts to grow cubic mixed phases by CVD have so far failed.

In this paper, the results of electronic structure calculations of the cubic $(BN)_x C_{2(1-x)}$ system are presented. This study complements a previous study of the diamond/c-BN heterojunction [9]. Our calculations address the question of the band gap behavior, the energy of formation and the phase stability. Rather restrictive but plausible assumptions are made about the short-range order in this alloy system.

The paper is organized as follows. Sec. II describes the computational approach. Sec. III describes the assumptions about the sort-range order. In section IV, we first discuss the results for the band gaps of the ordered compounds, next the phase diagram of the alloys, and finally, the properties of the disordered alloys. The conclusions of this work are summarized in Sec.V.

II. COMPUTATIONAL METHOD

The results presented here were obtained using Andersen's linear muffin-tin orbital method (LMTO) in the atomic sphere approximation (ASA) including the so-called combined correction [10]. The Kohn-Sham local density functional theory [11] is used with the exchange-correlation parametrization of Hedin and Lundqvist [12].

The local density approximation (LDA) is well known to underestimate the band gaps because the Kohn-Sham eigenvalues are not strictly speaking quasiparticle excitation energies. In this work, we estimate the quasiparticle self-energy correction using an expression derived by Bechstedt and Del Sole [13]. The latter is based on an approximate treatment of Hedin's GW approximation [14]. In Bechstedt and Del Sole's treatment [13], local field effects are neglected and matrix elements are calculated with a simple tight-binding approximation to the LDA wave functions. In the final closed expression of the correction,

$$\Delta = \frac{q_{TF}/\epsilon_\infty}{1 + \frac{7}{8} q_{TF} r_{sf}} \tag{1}$$

only well-known quantities appear such as the dielectric constant ϵ_∞, the Thomas-Fermi screening wave vector q_{TF}, and $r_{eff} = [(1 - \alpha_P)r_A/2 + (1 + \alpha_P)r_B/2]$ with r_A and r_B effective radii of cation and anion Slater orbitals given by $r_{A/B} = a/4\pi(1.7 \mp 0.05|Z_A - Z_B|)$ with a the cubic lattice constant and the bond polarizabilities α_P based on Harrison's universal tight-binding theory [15].

Our approach to studying the disordered alloys involves two parts. The first is the calculation of properties of ordered compounds representative of the assumed short-range order. In the second part, the statistically averaged properties of the disordered alloys are determined by a cluster expansion whose coefficients are derived by a mapping of the cluster expansion to the ordered crystal results. This is a generalization of the Connoly-Williams approach[16]. In the following section, we discuss our assumptions about the short-range order and the choice of ordered structures.

III. MODEL OF SHORT-RANGE ORDER

The short-range order in teterahedrally bonded heterovalent ternary alloys, of which the presently studied C-BN system is a particular case, has been discussed vigorously in a set of papers mostly in the middle 80's. Extensive experimental and theoretical studies were devoted to $(GaAs)_x Ge_{2(1-x)}$, $(GaSb)_x Ge_{2(1-x)}$ [17–26]. A recent overview of the field can be found in Ref. [26].

In the dilute limit of the III-V component in the alloy, one may expect isolated group-III and group-V impurities in a diamond lattice. That is, one can expect group-III and group-V elements to occur on either of the two fcc-sublattices of the diamond lattice with equal probability. At a higher concentration of the III-V component one may expect a transition to a nominally zinc-blende lattice in which the group-III element has a statistical preference for one of the sublattices and the group-V element for the other. The simplest way to view this transition is as a percolation problem [18]. More sophisticated treatments will include energetic and/or surface growth considerations.

From an energetic point of view, one may expect that the group-III and group-V elements would tend to be nearest neighbors. This is because the III-IV and IV-V ($\Delta Z = \pm 1$) bonds are under- and oversaturated respectively by 1/4 electron/bond. One thus can gain up to ~1/4 of the bandgap E_G by charge transfer from one to the other. This compensation leads to charged *donor* and *acceptor* bonds which costs electrostatic energy. As a result, the compensation is most effective for nearest neighbor III-IV and IV-V bonds in which case the electrostatic energy cost is minimized. These compensation effects between over-and undersaturated bonds have been discussed by Dandrea et al. [27] and Lambrecht et al. [28].

For similar electrostatic reasons, $\Delta Z = \pm 2$ bonds (V-V and III-III) are unlikely to occur. These basically correspond to antisite defects, which have a large energy of formation [29]. The same conclusion is reached from a study of inversion domain boundaries in GaAs [28]. In the case of the Ge-based alloys, there has been a controversy over the presence or absence of the $\Delta Z = \pm 2$ so-called "wrong" bonds [20, 22]. It was shown by Holloway and Davis [22] that their presence in any significant amount would lead to a closure of the gap because of the associated deep levels. This would be in disagreement with the experimental data on the bandgap behavior in these alloys and this was used as an argument for their absence.

Osório et al. [26] included the above mentioned electrostatic effects explicitly in a statistical thermodynamics treatment of these alloys. They concluded that the electrostatic effects tend to stabilize the zinc-blende ordering over the diamond structure. Below the melting temperature, however, both phases were found to be unstable towards phase separation over most of the composition range. The energetic arguments against the $\Delta Z = \pm 2$ bonds and for the "clustering" of $\Delta Z = \pm 1$ bonds are even stronger for compounds with larger ionicity and thus are more compelling for c-BN than for the GaAs and GaSb cases studied earlier.

From Badzian's X-ray diffraction studies [5], it appears that at least partial zinc-blende ordering can be assumed for the solid solutions of cubic C-BN prepared by him. That is, the B and N ions maintain a preferential occupation on separate fcc sublattices of which a certain percentage are replaced by carbon atoms in the mixed crystal.

In view of the above, we assume that the short-range ordering is characterized by (1) absence of B-B and N-N bonds, and (2) nearest neighbor positioning of B and N leading to local compensation of B-C and N-C bonds. These plausible assumptions correspond basically to assuming an almost perfect local *charge neutrality* and local *stoichiometry*. Obviously, this cannot be strictly applicable in the dilute limit of small x in $(BN)_x C_{2(1-x)}$. We choose here not to treat the controversial subject of the zinc-blende-to-diamond transition. Rather, we focus on the coarser problem of the miscibility and the properties of the most plausible short-range order structure over most of the composition range (excluding $x \ll 1$), which, as argued above, has the zinc-blende structure.

As a starting point, we study hypothetical ordered structures based on the zinc-blende structure. The models we investigated correspond for $x = 0.5$ to the $L1_0$ and for $x = 0.25$ and $x = 0.75$ to the $L1_2$ fcc-superlattices of BN and C_2 "molecules" oriented along the (111) direction. Of course, this does not imply that we atttach a meaning to these molecules as independent or weakly interacting entities. The system obviously is not a molecular crystal. This choice corresponds to the Connolly-Williams (CW) [16] $B_n C_{4-n}$ structures with $n \in \{0, 1, 2, 3, 4\}$ on one of the

fcc-sublattices. In each of these, there occurs exactly one type of the B_nC_{4-n} fcc-nearest neighbor tetrahedra. These tetrahedra form the basis of the cluster expansions used for the statistical tratment of the disordered alloys. For the purpose of statistically averaging the properties of the alloys, there is a one-to-one correspondence between the five basic tetrahedra and the five CW-structures.

IV. RESULTS

A. Band gaps of ordered compounds

We start with a discussion of the band gaps of the pure materials. The bandgap of c-BN has been somewhat controversial in the past because of the difficulty of obtaining single crystals of adequate size. A value of 6.4 eV as obtained by absorption measurements by Chrenko [30] on high-pressure synthesized cyrstals [31]. Recently, Mishima [32] measured the optical absorption edge to be 6.1 ±0.2 eV. Our previous calculations yielded a band gap of 4.46 eV within LDA and 6.4 eV including the Bechstedt-Del Sole correction. The band gap of diamond obtained by the same computational approach was 5.6 eV (4.1 eV in LDA) in fair agreement with the experimental value of 5.5 eV. From our and their experience, the Bechstedt-Del Sole approach is usually found to give a slight overestimate with errors of the order of a few 0.1 eV at most.

Based on the fact that the band gap of c-BN is larger than that of diamond, one might expect that mixed diamond-c-BN crystals would have band gaps larger than that of diamond. The calculated band gaps of ordered compounds are shown in Fig. 1. The LDA values are indicated by squares, the corrected values [33] by diamonds. Contrary to simple expectations, one sees that the gap initially shows a dramatic decrease upon alloying c-BN into diamond. Even for the 75 % c-BN compound, the gap is smaller than that of diamond.

We believe that the reason for this anomalously strong bowing of the bandgap can be understood in terms of the alignment of the energy bands in c-BN and diamond. As was shown in our earlier work on the heterojunctions between these two solids, the band offset is of the so-called type-II, (i.e. staggered type), as shown in Fig. 2. This means that the valence-band maximum of the composed system (mixed crystal or heterojunction) is mainly C-like while the conduction-band minimum is mainly BN-like with, in fact, a significant B-component because of the cation nature of the latter. This implies that the effective band gap of the system is lower than that of either of the two pure materials. The effect, in fact, is slightly more pronounced in the $L1_0$ structure studied here, which is a 1 + 1 (001) superlattice, than it is in larger period superlattices approaching the semi-infinite heterojunction [9]. This effect clearly may be expected to occur in other alloy systems in which the heterojunctions between the two constituent semiconductors is of type II, e.g. SiC/BP [34].

B. Phase stability

As already mentioned, it is not clear that this system is a true solid solution in the thermodynamic sense. First of all, this appears not to be the case for the other heterovalent ternary alloy systems, and secondly one may expect phase separation on the basis of the high interface energy of formation that we previously calculated for the heterojunction [9]. We discuss the miscibility phase diagram here within a very simple approximation.

First, in accordance with the assumptions about short-range order discussed in Sec. III, we treat the alloy-problem as a pseudobinary system of BN and C_2 "molecules". Secondly, the total energy of the solid solution is expanded in a cluster expansion using the above described fcc-tetrahedron approximation. The cluster energies are identified with the energies of formation of the corresponding CW-structures as explained in Sec. III.

For simplicity, we ignore the small lattice mismatch (~ 1 %) between diamond and c-BN. Thus we only need the energy of formation at their equilibrium volume. These are found from our first-principles total energy calculations to follow a parabola very closely, that is

$$\Delta H_o(x) = 4\Delta H_2 x(1-x) \tag{2}$$

with ΔH_2 the energy of the $L1_0$ compound equal to 0.45 eV/atom. The subscript "o" stands for "ordered" compound as opposed to the disordered alloys. While in general the CW-cluster expansion is equivalent to a *generalized* Ising spin model including triplet and tetrahedron interactions, the special case of a parabolic dependence on x is well known to correspond to the Ising model with only nearest neighbor pair interactions,

$$H = -\sum_{(ij)} J_2 S_i S_j . \tag{3}$$

In the present case, $J_2 > 0$ since like "molecules" prefer each other over unlike ones as nearest neighbors. This

is indicated by the positive energy of formation of the compounds. This means that the alloy statistics in this approximation is mapped on that of the well known ferromagnetic Ising model.

We briefly recall the "regular solution" or mean-field treatment of this problem. In this model, the entropy of mixing is approximated by the point-approximation in which $S = -k[x \ln x - (1-x)\ln(1-x)]$ with k the Boltzman constant. The free energy becomes $F(x,T) = \Delta H_o(x) - TS(x)$. At low temperature, this function shows a maximum at $x = 0.5$ and two minima symmetrically located on either side as shown in Fig. 3. With increasing temperature, the two minima converge towards the maximum until above a certain critical temperature, T_{MG}, they merge together in a single minimum at 50 %. The locus of these minima in the $x-T$ plane describes the miscibility gap (binodal line) and is given by

$$kT/\Delta H_2 = (8x-4)/[\ln x - \ln(1-x)]. \tag{4}$$

The region where $d^2F/dx^2 < 0$ is unstable and is bounded by the spinodal line

$$kT/\Delta H_2 = 8x(1-x). \tag{5}$$

The critical temperature $T_{MG} = 2\Delta H_2/k \approx 7700$ K.

The ferromagnetic Ising model has been treated by means of more sophisticated statistical methods, such as Kikuchi's cluster variation method (CVM) [35, 36]. With increasing size of the clusters taken into account in the entropy expression, one obtains a decreasing correction factor of 0.835-0.830 for T_{MG} relative to that for the regular solution approximation. The most accurate value known for the critical temperature was obtained by a high-temperature expansion [37] which gives the critical temperature as 0.81627 times the critical temperature of the regular solution model. Even with this correction factor, $T_{MG} \approx 6300$ K.

This is much higher than the melting temperature, which was estimated to be ~3500 K for c-BN and ~4000 K for diamond at ~10 GPa[1]. A tentative phase diagram including the renormalization of the critical temperature and the position of the liquidus line is shown in Fig. 4(a). As can be seen, our model predicts very limited mutual solubility of c-BN and diamond in the solid state, in apparent conflict with Badzian's claim of having synthesized solid solutions of compositions $0.15 < x_{BN} < 0.6$.

We next consider possible improvements to the simplified treatment given above. Including the lattice mismatch of about 1 % requires expanding diamond and compressing c-BN to the common lattice constant of the mixed crystal which will cost an additional energy ΔE_e. This should be followed by a relaxation of the bond lengths in the alloy, releasing an energy ΔE_r. These two effects partially cancel each other. We estimate that this may change the energies of formation and thus the temperature scale by at most a few percent. This would thus not alter our conclusion that the miscibility critical temperature lies well above the melting temperature.

A more important consideration might be the inclusion of long-range correlations. In some common-anion pseudobinary systems, this has been shown to lead to lowering of the miscibility critical temperature by as much as 60 % [38]. A renormalization of this magnitude would bring T_{MG} down to the order of the melting temperature. In particular, the fourth nearest neighbor pair interaction, which is between cations linked along the bond-chains in the (110) direction, was found to be quite important in Ferreira et al.'s [38] work. Since this has been found to be a rather general feature [38, 39], a similar effect may well occur in the present system. For the purpose of illustrating the following discussion, we show in Fig. 4(b) another tentative phasediagram which includes a 60 % renormalization due to these effects.

A complete treatment of long-range effects is beyond the scope of the present paper. Such a treatment should probably be based on extensions of the Blume-Emery-Griffiths $S = 1$ spin Hamiltonian [40] which was first applied to the problem of heterovalent ternary (III-V)-IV alloys by Newman et al. [20]. The generic phase diagram of this model Hamiltonian is characterized by the presence of a miscibility gap and an order-disorder transition between the zinc-blende and diamond phases in the solid solution region above the miscibility gap which ends at the binodal line in a tricritical point. We have thus tentatively indicated a zinc-blende-to-diamond transition in Fig. 4(b) with the understanding that the position of the transition is, of course, not known at this point, as is indicated by the question mark. We tentatively placed the line close to the diamond limit because Badzian's [5] results indicate that at least partial zinc-blende ordering was present in his samples down to $x = 0.15$. We emphasize that the form of the phase diagram shown here is very schematic. See for e.g. the papers of Newman et al. [20] and Osório et al. [26] for realistic phase diagrams of the $S = 1$ Hamiltonian for various values of the relevant parameters.

In the situation depicted by Fig. 4(b), one may imagine quenching the system from above the miscibility gap to lower temperatures. Above the miscibility gap, but below the melting line, the system would either have the diamond or zinc-blende —depending on which side we are of the order-disorder transition line— solid solution phase as thermodynamic equilibrium state. The corresponding phase would thus be frozen in at low temperature. The argument behind this is that at temperatures low with respect to the melting point phase separation would be

hindered by kinetic barriers which we will see are large. In a slight variation of this picture, one imagines the order-disorder transition line continued inside the miscibility gap as a metastable transition. In that case, if we are at a point vertically below a thermodynamic equilibrium zinc-blende phase, but on the left of the metastable transition line, the diamond phase would have a lower free energy than the zinc-blende phase, even though both have higher free energies than the phase separated state. The argument that such a transition could occur is that the change from zinc-blende to diamond ordering requires only local rearrangement of the atoms. This is less hindered by kinetic barriers than is phase separation. Of course, the speed at which the temperature of the system is lowered could determine which of the the two outcomes prevails.

We note that there has been significant controversy regarding this picture in either of its two variants. A proposed alternative theory is that the order-disorder transition between the diamond and zinc-blende phases, found experimentally for the Ge-based alloys, is purely of surface growth kinetic origin [21,22]. Still another possibility suggested by Osório et al. [26] but remaining to be explored is that a surface thermodynamic equilibrium phase gets frozen in because of absence of full bulk thermodynamic equilibration.

One way to test the validity of the "bulk thermodynamic" approach to this problem is to calculate the relevant interaction parameters from first-principles. There have only been limited attempts to calculate the interaction parameters of the $S = 1$ Hamiltonian from electronic structure calculations. The existing calculations [24–26] lead to parameters which would give a very high miscibility temperature (significantly higher than the liquidus line). Those results are similar to our present findings for the C-BN system. Osório et al. [26] found this to be true even when $\Delta Z = \pm 2$ bonds were excluded and the electrostatic and $\Delta Z = \pm 1$ compensation effects were taken into account as, in effect, has been done in the present work by our assumptions about short-range order. Now, a miscibility gap temperature above the melting point, as depicted in Fig. 4(a), makes the scenario of quenching in the zinc-blende form from a high temperature solid solution impossible. This fact lends indirect support to the idea that surface (kinetic or pseudo-equilibrium thermodynamic) effects need to be invoked to explain the zinc-blende ordering. Indeed, a miscibility gap temperature above the melting temperature would indicate that the mixed crystals or alloys can only be formed by condensation or solidification of a mixed gas or liquid phase in which, of course, a zinc-blende ordering does not make sense.

The "solid solutions" of c-BN-diamond obtained in Badzian's work [5] were obtained by direct (i.e. non-catalytic) solid state transformation of hexagonal C-BN crystals (obtained by CVD) at high temperature > 3300 K and pressures of $\sim$ 14 GPa. As stated in the paper, temperatures above the melting temperature may have occured in the center of the sample. Thus, the synthesis of mixed crystals does not contradict our prediction of the miscibility gap temperature being above the melting point.

In summary, by analogy to the more extensively studied Ge-based ternaries, the phase diagram of Fig. 4(a) following directly from our calculations, appears more likely than that of Fig. 4(b). Nevertheless, we note that none of the calculations of heterovalent ternaries so far has included the type of long-range effects which were found to be important for common-anion pseudobinaries. We can thus not completely exclude the situation indicated in Fig. 4(b). The experimental evidence is at present insufficient to distinguish between the two pictures.

Relaxing some of the assumptions about short-range order in our treatment (e.g. the requirement that B and N always occur as nearest neighbors) would introduce configurations of higher energy and thus presumably *increase* T_{MG}. Only the existence of special long-range order would seem to allow for an appreciable lowering of T_{MG}. Even with a lowering of T_{MG} by 60 %, it does not lie much lower than the liquidus. The conclusion of limited miscibility at reasonably low temperatures would thus remain valid even in this case.

Although the C-BN alloys are thus "in principle" unstable towards phase separation at room temperature, it can easily be seen that alloys are hindered from phase separating by large kinetic barriers. Indeed, we note that phase separation would require bond breaking and substantial diffusion. Since the bond-strengths are of the order of 4 eV, kinetic barriers will be huge compared to the "driving force" towards phase separation. The latter can be identified with the energy of formation which is an order of magnitude smaller as mentioned above.

For all practical purposes, these mixed crystals thus appear like true solid solutions even though they are in principle metastable. As is well known, this system is in addition metastable towards the hexagonal layered phases at ambient pressure.

C. Properties of disordered alloys

The properties of the disordered alloys such as the energy of formation and the bandgap can be expanded in a cluster expansion. We note that within the CVM one might calculate the probability distribution of the tetrahedral clusters from the energy minimization of the free energy. These may deviate from the random (binomial) distribution.

However, since the miscibility gap critical temperature is rather uncertain, as was discussed above, and the mixed compounds are, in fact, likely to have been formed in the liquid state, the use of a random distribution for statistical

averaging seems appropriate here.

For the energy of formation, this averaging leads to

$$\Delta H_d(x) = \sum_{n=0}^{4} \binom{4}{n} x^n (1-x)^{4-n} \Delta H_o(\tfrac{n}{4}), \tag{6}$$

$$= 3\Delta H_2 x(1-x). \tag{7}$$

where the energy of formation of the ordered compounds $\Delta H_o(\frac{n}{4})$ was substituted from Eq. (2). This statistical averaging is seen to lead simply to a renormalization by a factor of 3/4.

For the bandgaps of the disordered alloys, we obtain in a similar fashion.

$$E_G(x) = \sum_{n=0}^{4} \binom{4}{n} x^n (1-x)^{4-n} E_G^{(n)}. \tag{8}$$

where $E_G^{(n)}$ is the bandgap of the n-th CW-structure associated with the coresponding tetrahedral cluster. As expected, the resulting band-gap bowing, shown in Fig. 1 by the full continuous line, while still being vey strong, is somewhat less pronounced than that of the ordered compounds. We note that the tetrahedron approximation used for our cluster expansion is probably less converged for the bandgaps than for the total energies.

V. CONCLUSION

The main finding of this work is that c-BN-diamond mixed crystals and alloys exhibit an anomalously large band-gap bowing, which we propose to be related to the staggered band-offsets at the corresponding heterojunction.

We also discussed the phase stability within the tetrahedron approximation of a cluster expansion. Our model of the alloys is based on the absence of B–B and N–N bonds (because of their expected high energy) and nearest neighbor clustering of B–C and C–N bonds to ensure local charge neutrality. Within this restrictive model for the short-range order, the problem can be treated as a pseudobinary alloy problem. The energies of formation within this model were found to map onto the ferromagnetic Ising model. Their values lead to the prediction that the miscibility gap temperature would be well above the liquidus line. Although this conclusion is in agreement with more complete treatments of other heterovalent ternary semiconductor alloy systems, some uncertainty remains with regards to this conclusion. Indeed, long-range correlations have not been taken into account in any of these treatments. These correlations have been found to lower the miscibility gap temperature by as much as 60 % in some common-anion semiconductor alloy systems. An alternative tentative phase diagram was constructed including such a renormalization. The experimental conditions in which the mixed crystals were synthesized could be consistent with either of the tentative phase diagrams of Fig. 4 although our analysis seems to favor Fig. 4(a). Further work will be required to sort out which of these two alternatives applies.

The "in principle" metastability of the system should, however, not be a practical impediment to their use and further study since kinetic barriers towards phase separation are expected to be huge, even at fairly elevated temperatures. We hope this study will lead to further experimental work on this system which could verify our predictions about the band gaps.

ACKNOWLEDGMENTS

We thank Dr. Carlos Amador for helpful discussions. This work was supported by the National Science Foundation — Materials Research Group (DMR-89-03527) and the Office of Naval Research (N-00014-89-J-1631).

[1] R. C. DeVries, "Cubic Boron Nitride: Handbook of Properties" General Electric Technical Information Series, Report No. 72CRD178, (Schenectady, 1972).

[2] J. C. Angus and C. C. Hayman, Science 241, 877 (1988).

[3] G. L. Doll, J. A. Sell, C. A. Taylor II, and R. Clarke, Phys. Rev. B 43, 6816 (1991).

[4] D. R. McKenzie, P. J. Martin, S. B. White, Z. Liu, W. G. Sainty, D. J. H. Cockayne, and D. M. Dwarte, in *Proceedings of the European Materials Research Society Conference, Strassbourg, 1987*, edited by P. Koidl and P. Oelhafen (1988), p. 203.

[5] A. R. Badzian, Mat. Res. Bull. 16 1285 (1981); A. R. Badzian, in *Advances in X-ray Analysis*, Vol. 31, edited by Charles S. Barrett, John. V. Gilfrich, Ron Jenkins, John C. Russ, James W. Richardsonjr, and Paul K. Predcki, (Plenum, New york 1988).

[6] T. Ya. Kosolapova, B. N. Makarenko, T. I. Serebryakova, E. V. Prilutskii, O. T. Khorpyakov, and O. I. Chenysheva, Poroshk. metall. 1, 27 (1971).

[7] R. B. Kaner, J. Kouvetakis, C. E. Warble, M. L. Sattler, and N. Bartlett, Mater. Res. Bull. 22, 299 (1987).

[8] A. Y. Liu, R. M. Wentzcovitch, and M. L. Cohen, Phys. Rev. B 39, 1760 (1989).

[9] W. R. L. Lambrecht and B. Segall, Phys. Rev. B 40, 9909 (1989); 41, 5409 (1990).

[10] O. K. Andersen, Phys. Rev. B 123060 (1975); O. K. Andersen, O. Jepsen, and M. Šob, in *Electronic Band Structure and its Applications*, edited by M. Yussouff, (Springer, Heidelberg, 1987).

[11] P. Hohenberg and W. Kohn, Phys. Rev. 136, B864 (1964); W. Kohn and L. J. Sham *ibid.* 140, A1133 (1965).

[12] L. Hedin and B. I. Lundqvist, J. Phys. C 4, 2064 (1971).

[13] F. Bechstedt and R. Del Sole, *Phys. Rev. B* 38, 7710 (1988).

[14] L. Hedin, *Phys. Rev.* 139, A796, (1965).

[15] W. A. Harrison, *Electronic Structure and Properties of Solids* (Freeman, San Francisco, 1980).

[16] J. W. D. Connolly and A. R. Williams, Phys. Rev. B 27, 5169 (1983).

[17] Zh. I. Alferov, M. Z. Zhingarev, S. G. Konnikov, I. I. Mokan, V. P. Ulin, V. E. Umanskiĭ, and B. S. Yavich, Fiz. Tekh. Poluprovodn. 16, 831 (1982) (English Transl. Sov. Phys. Semicond. 16, 532 (1982); Zh. I. Alferov, R. S. Vatanyan, V. I. Korol'kov, I. I. Mokan, V. P. Ulin, B. S. Yavich, and A. A. Yakovenko, Fiz. Tekh. Poluprovodn. 16, 887 (1982) (English transl. Sov. Phys. Semicond. 16, 567 (1982).

[18] M. I. D'yakonov and M. É. Raĭkh, Fiz. Tekh. Poluprovodn. 16, 890 (1982) (English transl. Sov. Phys. Semicond. 16, 570 (1982).

[19] A. I. Gubanov and A. M. Polubotko, Fiz. Tekh. Poluprovodn. 16, 840 (1982) (English transl. Sov. Phys. Semicond. 16, 537 (1982).

[20] K. E. Newman, A. Lastras-Martinez, B. Kramer, S. A. Barnett, M. A. Ray, J. D. Dow, J. E. Greene and P. M. Raccah, Phys. Rev. Lett. 50, 1466 (1983); K. E. Newman and J. D. Dow, Phys. Rev. B 27, 7495 (1983); B.-L. Gu, K. E. Newman, and P. A. Fedders, Phys. Rev. B 35, 9135 (1987); A Kobayahi, K. E. Newman, and J. D. Dow, Phys. Rev. B 32, 5312 (1985).

[21] E. A. Stern, F. Ellis, K. Kim, L. Romano, S. I. Shah, and J. E. Greene, Phys. Rev. Lett. 54, 905 (1985); K. Kim and E. A. Stern, Phys. Rev. B 32, 1019 (1985).

[22] H. Holloway and L. C. Davis, Phys. Rev. Lett. 53, 830 (1984). L. C. Davis and H. Holloway, Phys. Rev. B 35, 2767 (1987).

[23] B. Koiller, M. A. Davidovich and R. Osório, Solid State Communn. 55, 861 (1985).

[24] M. A. Davidovich, B. Koiller, R. Osório, and M. O. Robbins, Phys. Rev. B **38**, 10524 (1988).
[25] T. Ito, Jpn. J. Appl. Phys. **26**, L1177 (1987); **27**, 1916 (1988).
[26] R. Osório, S. Froyen, and A. Zunger, Phys. Rev. B **43**, 14055 (1991).
[27] R. G. Dandrea, S. Froyen, and Z. Zunger, Phys. Rev. B **42**, 3213 (1990).
[28] W. R. L. Lambrecht, C. Amador, and B. Segall, Phys. Rev. Lett. **68** 1363 (1992).
[29] G. A. Baraff and M. Schlüter, Phys. Rev. B **33**, 7346 (1986); Phys. Rev. Lett. **55**, 1327 (1985).
[30] R. M. Chrenko, Solid State Communn. **14**, 511 (1974).
[31] R. H. Wentorf, Jr. J. Chem. Phys. **26**, 956 (1957).
[32] O. Mishima, in *Diamond, Silicon Carbide and Related Wide Bandgap Semiconductors*, Mater. Res. Soc. Symp. Proc. Vol. 162, edited by J. T. Glass, R. Messier, and N. Fujimori, (Mater. Res. Soc., Pittsburg PA, 1990), p. 543.
[33] For systems of about constant density, the self-energy correction Δ is approximately inversally proportional to the dielectric constant, (in this case, $\Delta \approx 8.3/\epsilon_\infty$ eV). We used 5.6, 4.5 and 6.5 as values of ϵ_∞ for diamond, c-BN and the alloys, respectively. The value used for the alloys is a rough estimate based on their smaller LDA band gap. This leads to values of Δ of 1.5, 1.9, 1.3 respectively.
[34] W. R. L. Lambrecht and B. Segall, Phys. Rev. B **43**, 7070 (1991).
[35] R. Kikuchi, Phys. Rev. **81**, 988 (1951); J. Chem Phys. **60**, 1071 (1974).
[36] J. M. Sanchez and D. de Fontaine, Phys. Rev. B **17**, 2926 (1978).
[37] D. M. Burley in *Phase Transitions and Critical Phenomena*, edited by C. Domb and M. S. Green, Vol. 2, (Academic Press, New York 1972), p. 329.
[38] L. G. Ferreira, S.-H. Wei, and A. Zunger, Phys. Rev. B **40**, 3197 (1989).
[39] A. Bieber and F. Gautier, Acta Metall. **35**, 1839 (1987); **34** 2291 (1986).
[40] M. Blume, V. J. Emery, and R. B. Griffiths, Phys. Rev. **4**, 1071 (1971).

FIG. 1. Band gap as a function of composition for zinc-blende derived $(BN)_x C_{2(1-x)}$ ordered crystals: LDA (squares), self-energy corrected [33] (diamonds) and random alloys (smooth full line).

FIG. 2. Band-offset at diamond-C/c-BN heterojunction.

FIG. 3. Free energy of $(BN)_x C_{2(1-x)}$ alloys within the regular solution model.

FIG. 4. Tentative phase diagrams of c-BN-diamond. (a) "Ferromagnetic Ising" model treated within regular solution

approximation renormalized by 82 % (b) same as (a) but including an *ad-hoc* 60 % lowering of the miscibility gap due to long-range correlations. A hypothetitical diamond (D) to zinc-blende (ZB) order-disorder transition is tentatively indicated with ? and dotted line. The liquidus line separating the liquid (L) from the solid portion of the phase diagram is indicated in both.

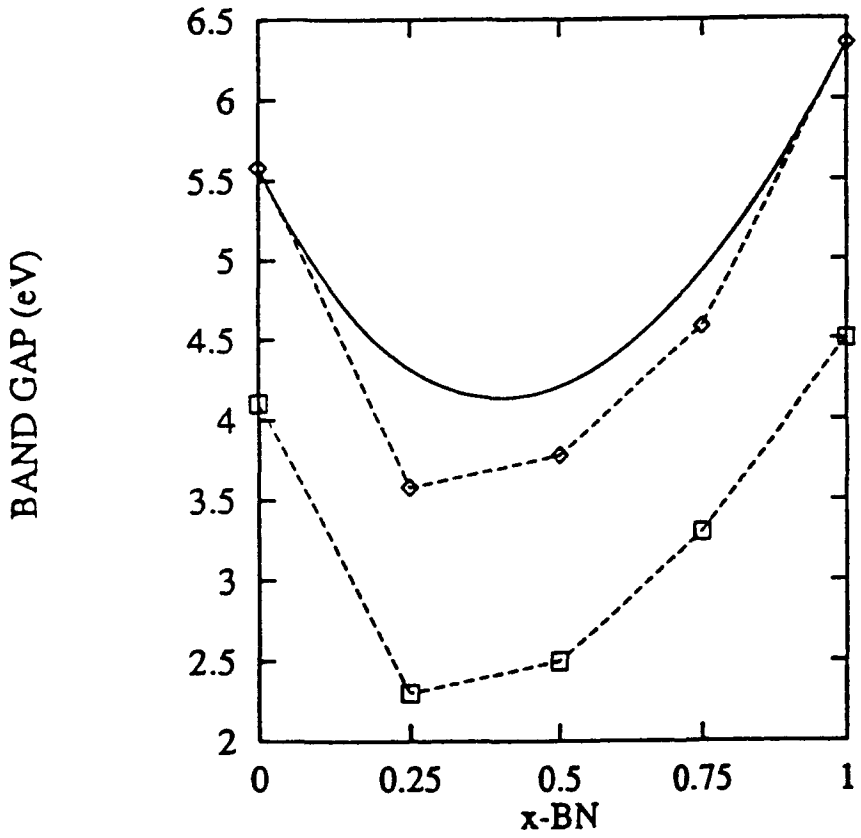
BAND GAP (eV)
6.5
6
5.5
5
4.5
4
3.5
3
2.5
2
0
0.25
0.5
0.75
1
x-BN

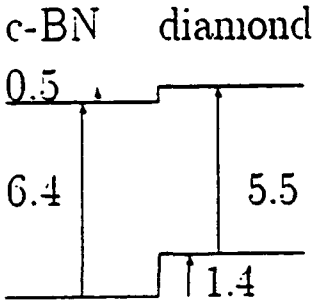
c-BN
diamond
0.5
6.4
5.5
1.4

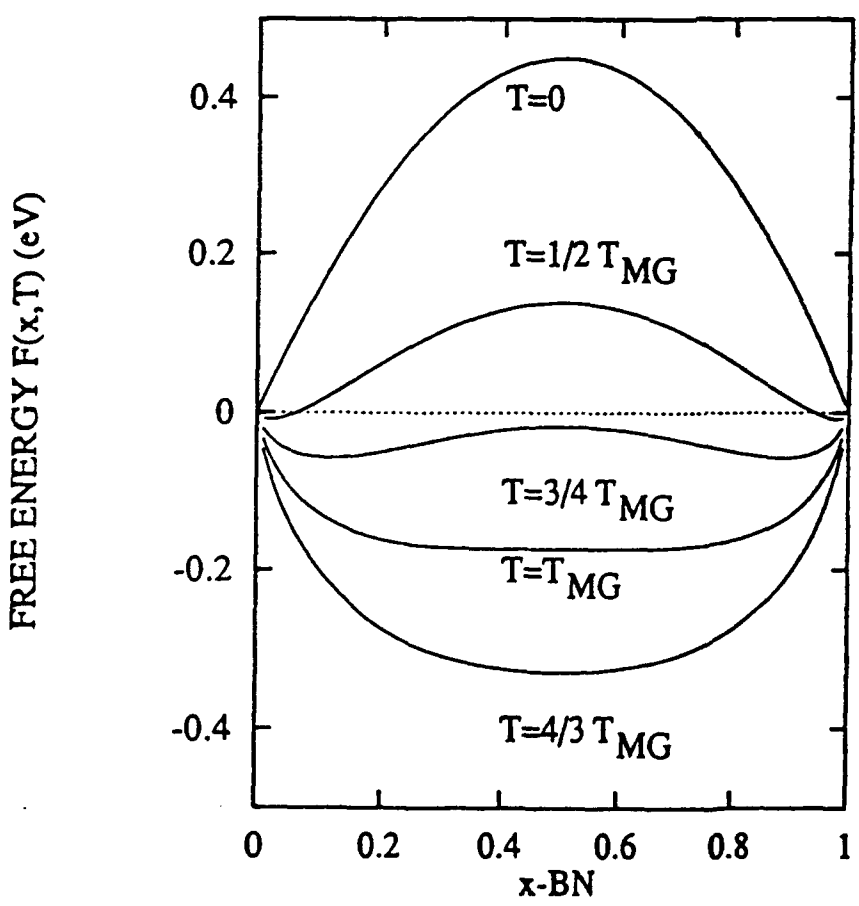
FREE ENERGY F(x,T) (eV)
0.4
0.2
0
-0.2
-0.4
T=0
T=1/2 T_MG
T=3/4 T_MG
T=T_MG
T=4/3 T_MG
0
0.2
0.4
0.6
0.8
1
x-BN

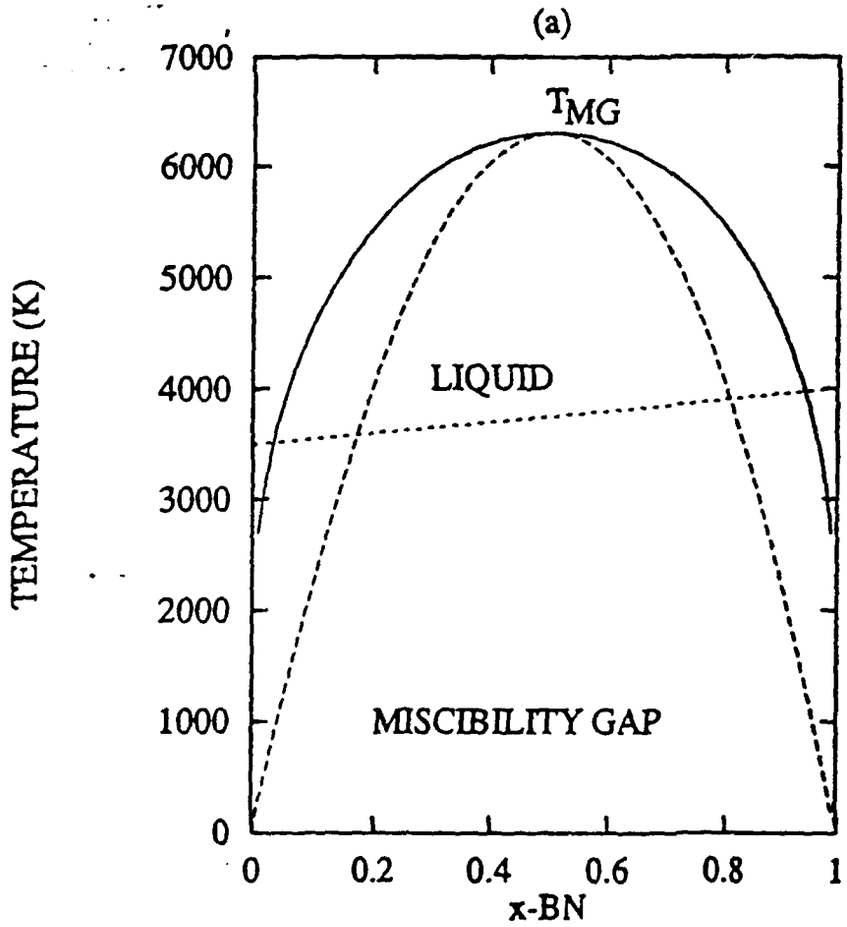
(a)
7000
6000
5000
4000
3000
2000
1000
0
TEMPERATURE (K)
T_{MG}
LIQUID
MISCIBILITY GAP
0
0.2
0.4
0.6
0.8
1
x-BN

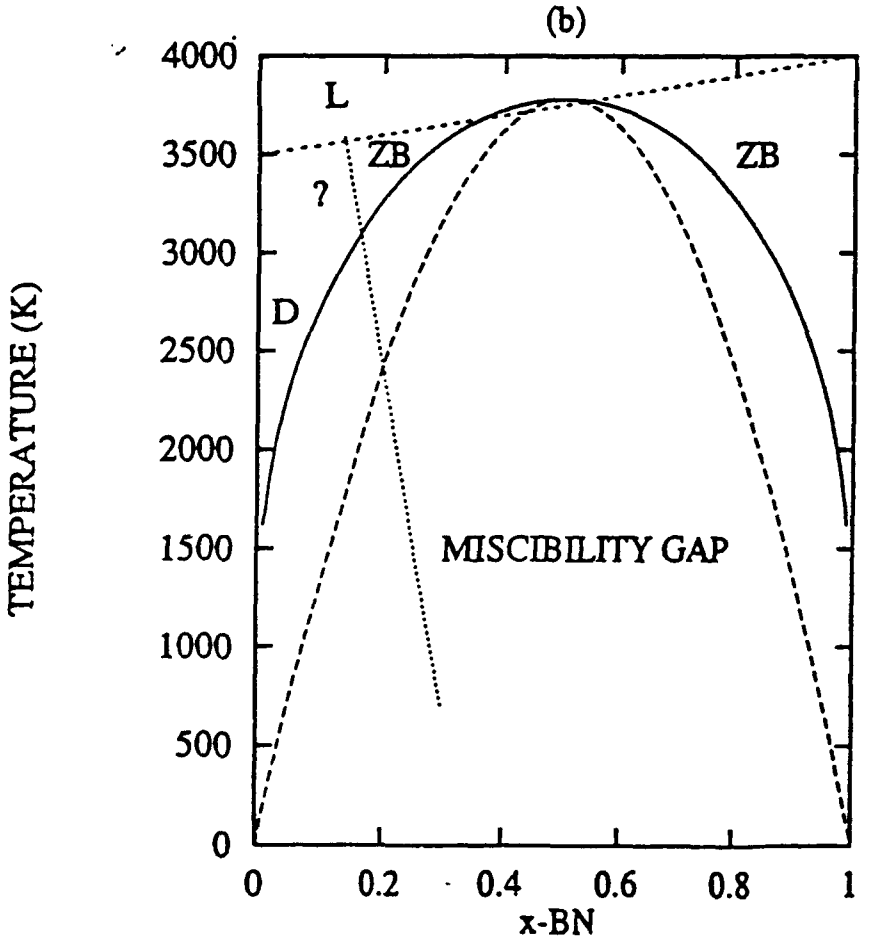
(b)
4000
3500
3000
2500
2000
1500
1000
500
0
L
ZB
ZB
?
D
MISCIBILITY GAP
0
0.2
0.4
0.6
0.8
1
x-BN
TEMPERATURE (K)